pH-responsive polymersomes for matrix metalloproteinase-1 delivery as a promising therapeutic strategy for the treatment of liver fibrosis

Eline Geervliet

Biomaterial Science and technology

Committee
Dr. Ruchi Bansal
Dr. Dietmar Appelhans
Dr. Ir. Jos Paulusse
Dr. Andries van der Meer

04-12-2019

Leibniz-Institut für Polymerforschung Dresden

UNIVERSITY OF TWENTE.

Preface

This is my thesis report with the title “pH-responsive polymersomes for matrix metalloproteinase-1 delivery as a promising therapeutic strategy for the treatment of liver fibrosis”. My thesis is performed in the Liver Lab, part of Biomaterials Science and Technology at the University of Twente. The research is a collaboration between the University of Twente and Leibniz Institute for Polymer Research, established by Ruchi Bansal and Dietmar Appelhans. Therefore, I want to thank Ruchi and Dietmar for making this possible. Besides, I want to thank Ruchi for her daily advice and guidance during my thesis and I want to thank Dietmar for his expertise and insights during my thesis. I also want to thank my other committee members Jos Paulusse and Andries van der Meer for being a member in my committee. Lastly, I want to thank Silvia for all her help, her contributions in sending all needed supply and her support during my thesis.

I couldn’t have achieved this without all the support of my friends and family. Therefore, I also want to thank my family and friends and especially Marco. Besides, I want to thank all my colleagues for their insights and help during my thesis and also for their support.

Table of content

Abbreviations

α-SMA	alpha smooth muscle actin
β-actin	beta actin
AB	antibody
ALD	alcoholic liver disease
ATRP	atom transfer radical polymerization
BCP	block copolymer
BLB	blue loading buffer
BMSC	bone marrow-derived stem cell
BrdU	bromodeoxyuridine
CCL_4	carbon tetrachloride
CLS	collagenase
CLS-1	collagenase type 1
Coll-1	collagen type 1
DDC	diethyldithiocarbamate
DDS	drug delivery system
DEAEMA	diethyl amino ethyl methacrylate
DLS	dynamic light scattering
DMEM	Dulbecco's modified Eagle's medium
DMIBM	3,4-dimethyl maleic imidobutyl methacrylate
DTT	dithiothreitol
EC	endothelial cell
ECM	extra cellular matrix
EPR	enhance permeability and retention
FBS	fetal bovine serum
H&E	hematoxylin and eosin
HCl	hydrochloric acid
HFF	hollow fiber filtration
HSC	hepatic stellate cell
IPF	institute for polymer research
MMP	matrix metalloproteinase
MMPsome	Psome decorated with MMP-1
MRI	magnetic resonance imaging
MWCO	molecular weight cut-off
NAFLD	non-alcoholic fatty-liver disease
NaOH	sodium hydroxide
NMR	nuclear-magnetic resonance
PBS	phosphate buffered saline
PDAC	pancreatic ductal adenocarcinoma
PDI	polydispersity
PEG	poly (ethylene glycol)

Psome	polymersome
PV	portal vein
qPCR	quantitative polymerase chain reaction
RhB	rhodamine B
TGF-β	transforming growth factor beta
THV	terminal hepatic vein
TIMP	tissue inhibitors of matrix metalloproteinase
US	ultrasonography

Abstract

Background & Aims: Liver fibrosis is a growing health problem affecting millions of people worldwide. Chronic liver injury leads to the formation of scar tissue due to the excessive accumulation of extracellular matrix, mainly collagen-I and -III produced by activated hepatic stellate cells (HSCs). Currently, there are no therapies available for liver fibrosis. Matrix metalloproteinase-1 (MMP-1) is an enzyme that degrades the scar tissue by degrading collagen-I and -III favoring fibrolysis. We hypothesized liver-specific delivery of MMP-1 to degrade collagen as a promising approach for the treatment of liver fibrosis. Using state-of-the-art technologies, we synthesized innovative pH-responsive smart MMPsomes with the MMP1 decorated on the polymersome surface. Finally, we investigated the therapeutic efficacy of MMP1 and MMPsomes on human HSCs *in vitro* and on liver fibrosis mouse models *in vivo*, and *ex vivo* on fibrotic mouse livers.

Methods: Polymersomes (Psomes) were fabricated using the pH switch method and MMP-1 post-loading at pH 5-6 was performed to increase the interaction between MMP-1 and the Psome membrane. Physiochemical analysis and enzymatic assays were performed to characterize the attachment and functionalization of enzyme on the Psomes. *In vitro* studies were performed on TGF-β activated human HSCs to evaluate the effects of MMP1 and MMPsomes on the cell viability, functionality and the gene and protein expression of collagen and HSCs activation marker α-SMA. Finally, the efficacy of MMP-1 and MMPsomes was tested *in vivo* and *ex vivo* on CCl_4-induced liver fibrosis mouse models

Results: Decoration of MMP-1 on the surface of the polymersome was successfully established with an affinity of 30%, without inhibition of function. Synthesized MMPsomes showed favorable size (~180nm at pH 6 and ~145 nm at pH 8) and charge (positive at pH 6 and negative at pH 8). MMP-1 and more significantly MMPsomes showed dose-dependent inhibition of collagen-I, -III and α-SMA gene expression, and collagen-I protein expression in TGF-β activated human HSCs with no significant effects on cell viability. The studies on CCl_4-induced liver fibrosis mouse models have been performed, showed promising preliminary results with no *in vivo* toxicity however still under investigation.

Conclusions: In conclusion, we present an innovative approach of MMP-1 delivery for the treatment of liver fibrosis.

1. Introduction

1.1 Epidemiology of liver fibrosis

Liver fibrosis is the characteristic change of healthy liver tissue into fibrous tissue, due to chronic liver injury (1). The age-adjusted prevalence of fibrosis in European countries varies from 447 to 1,100 per 100,000 with a median of 833, mainly caused by excessive alcohol abuse or hepatitis B/C infection (2,3). Liver fibrosis is responsible for 1.8% of all deaths in Europe (4). In developed countries alcoholic liver diseases (ALDs) are the biggest cause of liver fibrosis, however, non-alcoholic fatty-liver diseases (NAFLDs) increase the prevalence (1–4). On the other hand, NAFLDs do not increase the mortality rate of liver fibrosis, since the direct cause of death of these patients is usually defined as heart and vascular diseases (2,3). The prevalence and underlying cause for most European countries is displayed in **Figure 1** (3).

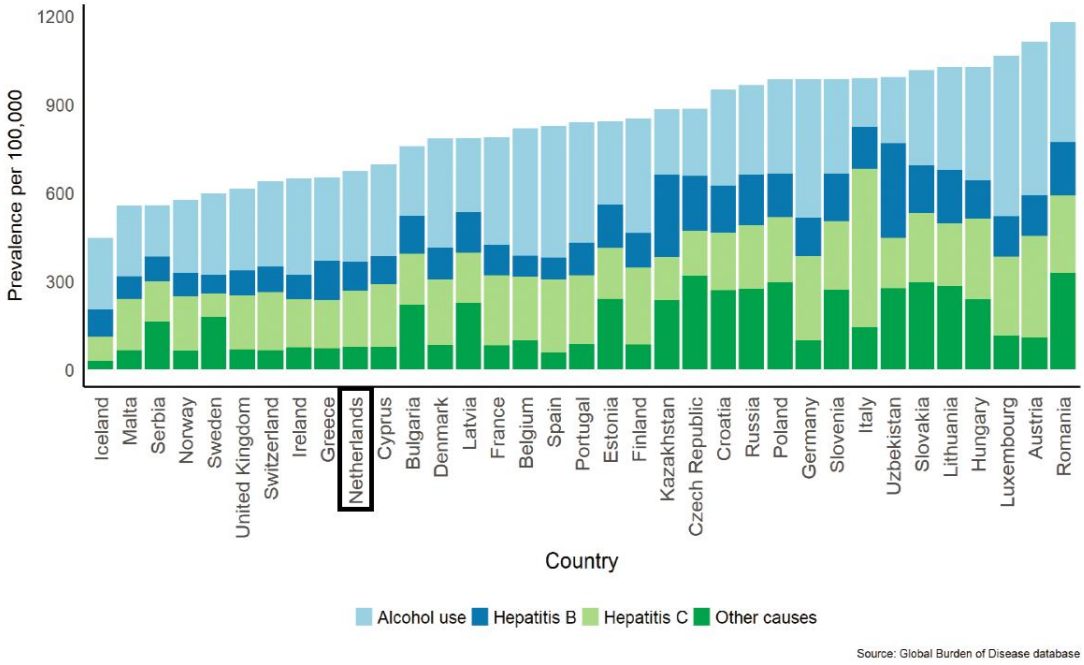

***Figure 1**. Age-standardized prevalence of liver fibrosis in Europe in 2016 [Pimpin_2018_project]*

1.2 Pathogenesis

The main function of the liver is blood purification by metabolism of carbohydrates, proteins and lipids and by detoxification and clearance of chemicals, drugs and other xenobiotic compounds. Besides, the liver is responsible for synthesis of different proteins (5). Hepatocytes are the cells mainly responsible for the metabolic function (1). In a healthy liver, blood flows from the portal vein (PV) to the terminal hepatic vein (THV), through a liver sinusoid. A sinusoid is a capillary surrounded by fenestrated endothelial cells that are supported by loose connective tissue called the space of Disse. Blood can pass through the fenestrations and reach the space of Disse. Here, hepatocytes are lined up to perform blood purification and secrete synthesized compounds. In the space of Disse, regulatory cells present, called hepatic stellate cells (HSCs) (1,5,6). HSCs in a healthy liver ensure vitamin A storage, maturation of hepatocytes, vasoregulation and homeostasis of the extracellular matrix (ECM) (6). ECM homeostasis is regulated by secretion of ECM proteins and remodeling enzymes, such as collagen, matrix metalloproteinases (MMPs), proteins that break down the ECM, and tissue inhibitors of matrix metalloproteinases (TIMPs) (5).

Fibrosis is defined by the replacement of healthy tissue by collagenous scar tissue due to increased production and decreased degradation of ECM (1,5). This disbalance is caused by chronic liver injury, such as ALD, NAFLD and hepatitis B/C (2,3). Due to chronic injury, hepatocytes go in apoptosis or necrosis and release various factors as reactive oxygen species, plasmin and acid (6). These factors, in turn, stimulate the activation of transforming growth factor beta (TGF-β) by TGF-β-binding protein (LTBP) and latency-associated peptide (LAP). Active TGF-β can induce a signaling pathway that targets fibrogenic target genes, which increase the release of alpha smooth muscle actin (α-SMA), collagen and TIMPs (7). This pathway is pictured in Appendix A, **Figure 22Figure 22** (7). When the TGF-β-SMAD pathway is stimulated chronically, it will lead to HSC activation (6,8). Upon activation, HSCs lose their ability to store vitamin A and transform into contractile myofibroblast-like cells. These HSC-derived myofibroblasts produce uncontrollable amount of collagen type 1 (coll-1), type 3 (coll-3) and TIMPs and reduce the secretion of MMPs. This disrupted balance between ECM composition and decomposition leads to fibrosis, the emerge of scar tissue (6,9–13). Due to the deposition of ECM, fenestrations between endothelial cells are lost, and hepatocytes become apoptotic, which leads to inhibition of blood clearance (6). The changes described here are visualized in **Figure 2**. Cirrhosis is the advanced state of fibrosis which is characterized by disrupted hepatic vasculature; blood flows without clearance from the PV to the THV, which leads to increased hepatic resistance and thereby to portal hypertension. Due to lack of blood clearance and increased portal pressure, cirrhosis eventually will lead to multiorgan failure (1,6,14).

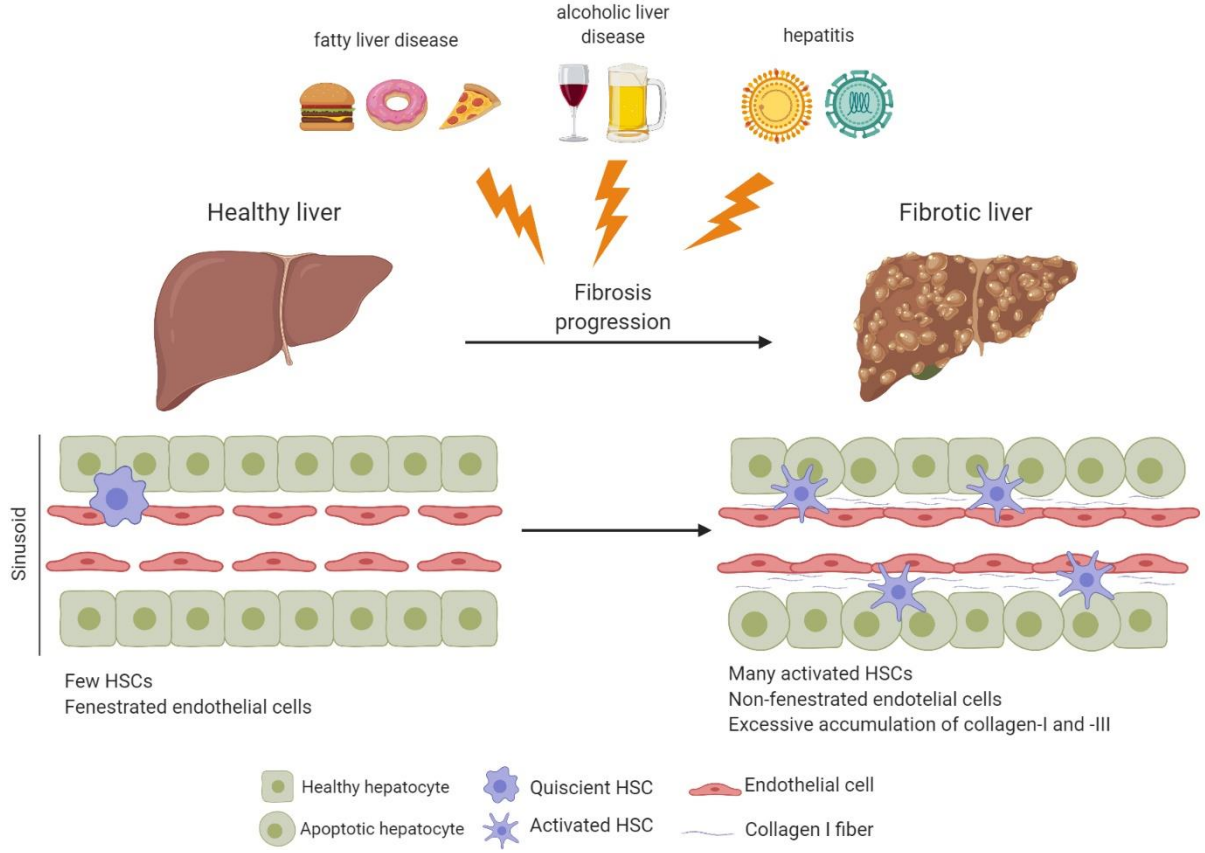

Figure 2. *Differences between a healthy and fibrotic liver. In a healthy liver, quiescent, vitamin A containing HSCs are pictured. Only a few HSCs are present in a healthy liver. Hepatocytes are neatly arranged alongside the blood vessel. Fenestrations between the endothelial cells allow metabolic exchange between blood and hepatocytes. Endothelial cells and hepatocytes are separated by loose ECM, called the space of Disse. In the fibrotic liver the HSCs are activated and proliferated, illustrated by the extended branches. The HSCs have promoted the increased deposition of coll-1 and coll-3 in the space of Disse. This change in ECM clogs the fenestrations and inhibits metabolic exchange between blood and hepatocytes. Also, the hepatocytes became apoptotic.*

1.3 Diagnosis and treatment

Different diagnostic methods include the use of laboratory biomarkers, imaging techniques and the golden standard of liver biopsy, all with their advantages and disadvantages (1,8,15). Liver biopsy is considered the golden standard for diagnosing and staging liver fibrosis. However, it can be difficult to stage fibrosis correctly, due to disease heterogenicity and inter-/ intra lobular variety. Besides, taken a biopsy is invasive and includes the risk of bleeding (1,8,15). Therefore, other diagnostic tools are developed, such as laboratory biomarkers. The laboratory biomarkers can be divided into fibrosis specific biomarkers, class I, and liver function biomarkers, class II. For the class I biomarkers, the outcome is very different depending on the underlying cause and therefore it is difficult to find a threshold at which fibrosis is established. Considering the class II biomarkers, they can be influenced by various unrelated diseases and lack specificity (8,15). For imaging, ultrasonography (US), computed tomography and magnetic resonance imaging (MRI) are used. However, since these techniques rely on structural and morphological changes, they are not sufficiently sensitive for the diagnosis of early stage fibrosis (1,8). Besides, US and MRI can be used to measure the perfusion of tissue surrounding the sinusoids. If (late-stage) fibrosis is present, perfusion of water molecules is inhibited by the dense and collagen rich ECM (8). Also, the diameter and velocity of the PV and THV can be measured, to screen for portal hypertension in end stage liver fibrosis (1). An upcoming and widely used method is to measure the stiffness of the liver with different types of transient elastography. Due to collagen accumulation in the liver, the liver stiffness is increased. US is used to measure the shear wave velocity, which correlates with the stiffness and thereby fibrosis of the liver (1,8). Even though, these measurements are promising and in specific cases can avoid invasive biopsies, they cannot provide detailed histological information (1,8,15).

Nowadays, the only successful treatment of (end-stage) liver fibrosis is liver transplantation, but due to a limited number of available donor organs, this solution is insufficient (8,14,16,17). Other treatments mainly focus on removing the underlying cause of fibrosis (1,8,14,15). For early-stage fibrosis this can slow the progression and even reverse the disease, in late-stage fibrosis however, removing the cause will not reverse the disease completely and is therefore insufficient. Other treatments are necessary (1,10).

1.4 Matrix metalloproteinases

As mentioned before, ECM remodeling is regulated by deposition of ECM and secretion of MMPs and TIMPs. A distorted balance between MMPs and TIMPs, in which the TIMPs are overexpressed favors fibrogenesis and is ascertained in fibrosis (5,9–11). To successfully remodel this fibrotic scar tissue, additionally to removing the underlying cause, degradation of the existing fibrous ECM is required (10,17). Since the discovery of the first MMP in 1962(18), 28 different MMPs are known, of which 23 are found in humans. These can be categorized in six different groups based on the substrate: the collagenases (MMP-1, MMP-8, MMP-13), the gelatinases (MMP-2, MMP-9), the stromelysins (MMP-3, MMP-10, MMP-11, MMP19), the matrilysins (MMP-7, MMP-26), the membrane-type MMPs (MMP-14, MMP-15, MMP-16, MMP-17, MMP-24, MMP-25) and others (MMP-12, MMP-20, MMP-22, MMP-23, MMP-28) (19). Different MMPs play a key role in the initiation, progression and resolution of liver diseases (19–21). These different roles are explained in Appendix B, **Table 2**. The first sub-class of MMPs is collagenase (CLS), which consists of MMP-1, MMP-8 and MMP-13. CLSs are known for their degrading ability of collagen (9). Of these MMPs, MMP-1 is the key player in degradation of coll-1 and collagen type 3, which are in turn the most abundant

ECM component in liver fibrosis (5,9–11,17). Therefore, different researchers focused on enhancing the MMP-1 level to attenuate liver fibrosis.

Iimuro et al. tried to restore the MMP-TIMP balance by promoting MMP-1 expression via recombinant adenovirus gene delivery in rats with thioacetamide induced hepatic fibrosis. They observed an attenuation of fibrosis after infection, detected by histological staining with Masson's trichrome. Also, a reduction of activated HSCs was visualized with α-SMA and collagen staining. At last, they observed and hepatocyte proliferation with bromodeoxyuridine (BrdU) and hematoxylin and eosin (H&E) staining (17). This is a promising cure to attenuate liver fibrosis. However, it should be born into mind that the use of viral vectors can have immunogenic and toxic effect. Also, when the vectors are used for a longer period, it is possible to induce an unwanted overexpression of MMPs which will lead to over-degradation of ECM (10).

Du et al. attempted to reverse fibrosis by treatment with MMP-1 expressing bone marrow derived stem cells (BMSCs). Firstly, they isolated the BMSCs of rats and transfected them with recombinant adenovirus vector containing human MMP-1. After establishment they compared the attenuation of fibrosis of the control, a CCl_4 fibrotic model, a BMSC treated model and a BMSC-MMP-1 transfected model. H&E staining was performed to evaluate the microscopic fibrosis, which was lower in the BMSC-MMP1 model than in the BMSC or the wild-type model. Moreover, the collagen amount lowered, concluded with a Masson staining, and the same accounts for hydroxyproline and α-SMA. Lastly, they tested different kind of fibrotic serum markers and concluded that BMSC-MMP-1 treatment is a promising treatment of liver fibrosis (14). On the other hand, the use of BMSC has some disadvantages. First of all, retrieving the cells is an invasive procedure (22). Besides, there is no optimized protocol for the delivery route, nor the number of injections (23).

Liu et al. tried to induce MMP-1 expression via activation of the Erk1/2 and Akt pathway. In their paper, they described the role of diethyldithiocarbamate (DDC) in the activation of ERK1/2 and Akt, which inhibit miR-222. This RNA is responsible for the inhibition of MMP-1 production. If miR-222 is inhibited, the production of MMP-1, is stimulated. Eventually they hypothesize that liver fibrosis can be treated with DDC via MMP-1 stimulation (11).

These researches explain to us that degradation of ECM is possible with MMP-1 and the degradation of ECM stimulates healthy regeneration of fibrotic liver tissue and proliferation of hepatocytes.

1.5 Drug delivery systems and polymersomes

The previous paragraphs demonstrated the fibrolytic effects of MMP-1 overexpression. However, stimulation of MMP-1 expression by gene therapy may lead to prolonged MMP-1 expression, which has carcinogenic effects (17). Gene therapy can be avoided by administration of MMP-1 without genetic modifications. Since MMP-1 is an enzyme and free enzymes are degraded within minutes in the body, MMPs need to be escorted by a drug delivery system (DDS). DDSs are synthetic carriers with enhanced stability in the bloodstream that deliver drugs or other compounds to a selective target, for example the liver (24).

Polymersomes (Psomes) are polymeric vesicles formed by self-assembly of amphiphilic block copolymers (BCPs). Psomes are ideal DDSs because of their tunability. Compared to their biological equal, the liposomes, Psomes have enhanced mechanical and chemical stability, increased surface functionality and

controllable pharmacokinetics (24–26). The assembly of polymersomes is driven by non-covalent forces like hydrophobic interaction, hydrogen bonds, electrostatic forces and Van der Waals interactions (25). To direct the self-assembly, different fabrication techniques are known, among which; direct hydration method, film hydration method, microfluidic directed assembly, solvent switch method and pH switch method (25–27). Direct hydration is a quick and straightforward fabrication method in which the BCP is directly added in an aqueous solution stimulating direct assembly. However, longer hydration time and high stirring speed, which may increase the polydispersity (PDI), are required (25,26). With the film hydration method, the BCP is dissolved in an organic solution which is slowly evaporated leaving a thin film of BCP. Rehydration is performed using an aqueous solution, resulting in self-assembly of Psomes (25–27). This method is typically used to form giant vesicles in the micrometer range (25). Microfluidic directed assembly is developed to create monodisperse and size controlled Psomes. The microfluidic method uses two phases, the organic phase which contains the BCP and the water phase. Formation is established using water in oil in water micro-emulsion, water is pushed through the oil phase and then through the water phase again, leaving monodisperse Psomes (25,26). For the solvent-switch method, the BCP is dissolved in a solvent that dissolves all the blocks of the BCP, this usually is an organic solvent. Then, while stirring, the BCP containing solvent is added to a solution that only dissolves one particular block, usually an aqueous solution. Afterwards the organic solvent is removed by dialysis (25–27). A sub-group of the solvent-switch method is the pH switch method. This can be used for BCPs with a pH sensitive block that can dissolve in low pH aqueous solutions, but is insoluble in high pH aqueous solutions. To induce self-assembly, the BCP is dissolved in a low pH aqueous solution and the pH is slowly increased while stirring. Due to the insolubility of the pH-responsive block, new hydrophobic interactions direct the Psome formation (25).

Gaitzsch et al. have fabricated a pH-sensitive, photo-crosslinked Psome. The pH-sensitivity leads to pH depending permeability while crosslinking inhibits the disassembly of Psome and provides higher mechanical and chemical stability. The Psome is assembled from specific BCPs containing the biocompatible, hydrophilic poly(ethylene glycol) (PEG), the pH responsive diethyl amino ethyl methacrylate (DEAEMA) and the photo-crosslinkable 3,4-dimethyl maleic imidobutyl methacrylate (DMIBM) (28,29). When the pH decreases, DEAEMA becomes protonated and therefore hydrophilic, resulting in the urge to disassemble into the medium. However, due to the crosslinked DMIBM, disassembly is prevented and the Psome swells instead. A schematic representation of the Psome is given in **Figure 3**.

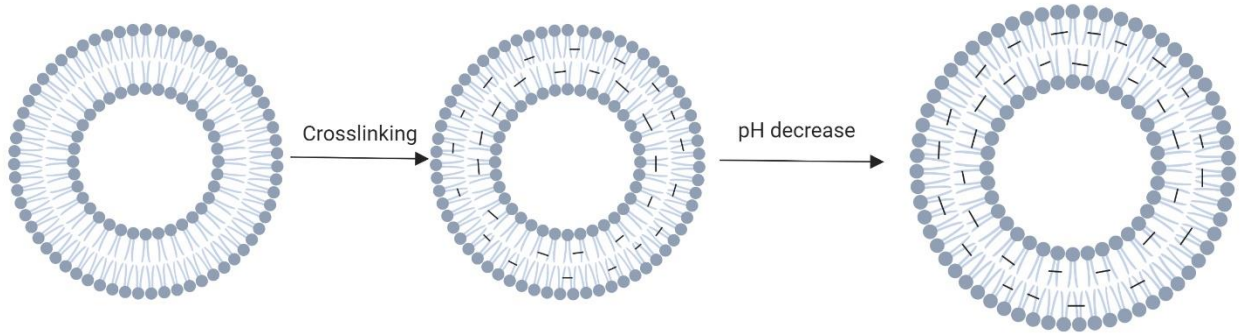

Figure 3. *Psome before and after crosslinking; the black lines visualize the crosslinking. Made with Biorender.*

At protonated state, the membrane is hydrophilic and allows exchange of small molecules (28,30). More research into the swollen and collapsed state has been performed. Gumz et al. demonstrated that the pH switch point of 6.6, is adjustable. When the original amount of 20 units DEAEMA is reduced and replaced by complete hydrophobic polymers, the pH switch point decreases. Gumz et al. managed to produce different BCPs that can provide a range of Psomes with a pH switch point starting from 5.1 till 6.8 (31). Moreover, this Psome is used for membrane functionalization and attachment of active targeting ligands. Conjugation of specific targeting ligands on the Psome can provide targeted delivery and thereby enhance therapeutic effect, combined with minimized side-effects. To successfully conjugate these ligands to the surface of the Psome, functionalization with reactive groups is necessary. Iyisan et al. demonstrated the functionalization of Psomes with amino groups to allow conjugation with biological entities, which allow active targeting (32). The functionality in drug delivery is also examined. Research has proved that this Psome can encapsulate one or more enzymes, without hampering the activity. Advantages of encapsulation are the guaranteed protection of the encapsulated compound by the Psome. However, when encapsulated a releasing step at the target site is required. The advantage of this specific Psome is easy encapsulation of small compounds at low pH, when the membrane is permeable and protection at physiological pH, when the membrane is collapsed (30,32).

2. Aim of the research

2.1 Aim and objectives

As discussed before no successful treatment for liver fibrosis available yet. The aim of our study is to provide a promising therapeutic strategy for the treatment of liver fibrosis by delivery of ECM degrading MMP-1 using a pH-responsive Psome.

To reach this aim we have formulated different objectives:

- Engineering and characterization of an MMP-1 containing Psome, the MMPsome;
- Evaluation of the toxicity of Psome and MMPsome;
- Evaluation of the *in vitro* therapeutic effect of MMP-1 and MMPsome;
- *In vivo* study on MMP-1 and MMPsome efficacy in CCl_4-induced acute fibrotic mouse model;
- *Ex vivo* evaluation of MMP-1 and MMPsome efficacy on fibrotic liver tissue ECM degradation.

2.2 Strategy

In this study we want to find a treatment for liver fibrosis based on MMP-1 delivery to restore the MMP-TIMP balance and fibrolysis. To overcome the degradation of MMP-1, we want to use the previously discussed Psome as DDS. Most studies have demonstrated encapsulation of enzymes in the lumen of the Psome (28,30,33,34). However, MMP-1 is oversized and therefore, not able to pass the membrane in protonated state. If encapsulated, an enzyme releasing step is necessary for enzyme activity (30,34). The Psome used in this experiment is chemically and mechanically stable, so a releasing step needs to be evaded. Therefore, we engineered a Psome with MMP-1 decorated on the outer surface of the Psome. The MMP-1 used in this research is CLS type 1 (CLS-1), received from Sigma Aldrich (35). During my internship at the Leibniz Institute for Polymer Research (IPF) in Dresden, this state-of-the-art research into the optimal fabrication protocol was performed and the MMPsome was characterized. The most important features, comprising successful decoration, decoration efficiency and MMP-1 activity changes due to decorations are discussed. The materials and methods used for the optimal decoration and purification protocol are explained and discussed. Furthermore, the decoration efficiency of the protocol is evaluated using fluorescent labeled MMP-1. Lastly, the activity of MMP-1 before and decoration is evaluated using a collagenase activity kit.

During my thesis assignment the next step to increase the clinical relevance is performed. *In vitro* studies on efficacy of the MMP-1 delivery is tested using LX-2 cell-line, a human HSC cell-line that can be activated using TGF-β into a fibrotic HSC model. Since HSCs are the major contributor to liver fibrosis, they are also the target cells for anti-fibrotic drugs (6,36). However, due to low availability of human HSCs and high impurities in the harvested cells, an established cell-line of human HSCs are essential for this research. Xu et al. compared two different cell-lines, LX-1 and LX-2, with the HSCs on desired features for anti-fibrotic therapy research. These cell-lines have higher availability and less frequent impurities. Key characteristics, such as activation upon TGF-β stimulation is found is both LX-1 and LX-2 cell-lines. Besides, the LX-2 cell-line is favorable due to the high transfectability of >30%, making gene therapy possible. So, due to the high availability and stability of LX-1 and LX-2 cell-line and the response to fibrotic stimulation, these cell-lines provide an ideal platform for anti-fibrotic therapy development (36). In this study, the LX-2 cell line is used. During the *in* vitro studies, the cell viability with different concentrations of MMP-1, Psome and MMPsome will be evaluated, using an Alamar blue assay. Furthermore, the efficacy of the treatment will be compared to a negative (non-activated) and positive (TGF-β activated) control. Efficacy of different concentrations

will be evaluated via the expression of fibrogenic genes using PCR and via the presence of fibrogenic proteins using western blotting. Furthermore, functionality tests are performed by a 3D-contractility assay and a 2D-scratching assay.

Lastly besides the *in vitro* studies, *in* and *ex vivo* to characterize the efficacy further, are performed using CCl_4 induced acute fibrosis mouse model. CCl_4 is a toxic compound which is metabolized in radicals that can react with different compounds and thereby induces hepatic damage, characterized by inflammation, fibrosis, cirrhosis and hepatic cellular carcinoma (HCC) (37). For time-management reasons, an acute study using CCl_4 is used. Here, the efficacy of MMPsome is compared to wild-type mice and free MMP-1 treated mice. Evaluation is performed by gene expression of fibrotic genes using PCR and immunohistochemical staining of liver section. Beside *in vivo* studies, sections fibrotic livers of wild-type mice are used for *ex vivo* treatment, Here the efficacy of MMPsomes on liver tissue is compared to non-treated liver tissue and free MMP-1 and Psome treated liver tissue. These studies combined form my master thesis and are elaborated explained in this report.

Chapter 3 Materials and methods

In this Chapter all the materials and methods are elaborately explained. First the materials and methods for the fabrication of MMPsomes used in Dresden at IPF are discussed in paragraph 3.1.

After this an elaborate list of materials used at the University of Twente for all *in vitro* and *in vivo studies* are displayed in paragraph 3.2, These studies will be discussed in the paragraphs that follow 3.2. Paragraph 3.3 and 3.4 are dedicated to the general work including preparation of different concentration of MMP-1, Psome and MMPsome and general cell culturing. Paragraphs 3.5 till 3.9 elaborately explain the different *in vitro* studies.

Lastly, paragraph 3.10 will be dedicated to the *in* and *ex vivo* studies.

3.1 MMPsomes

3.1.1 materials used at IPF, Dresden

BCP: PEG_{45}-b-($DEAEMA_{75}$-s-$DMIBM_{20}$); hydrochloric acid (HCl) (Merck); sodium hydroxide (NaOH) (Sigma); OmniCure® S2000 spot UV curing lamp system (Lumen Dynamics Group Inc., Canada); A Zeta-sizer Nano-series instrument (Malvern Instruments, UKK); MMP-1: collagenase type I, prepared from Cl. Histolyticum (Sigma-Aldrich, C0130-100mg, CAS nr 9001-12-1); 1000 kDa MWCO membrane (Spectra/Por® Membrane, Biotech CE Tubing); phosphate buffered saline (PBS) tablets (Sigma Aldrich).

3.1.2 Fabrication of MMPsomes

Fabrication of the Psome was done according to previously published methods of Gaitzsch et al. (28). For the fabrication of a pH responsive photo-crosslinked Psome solution of 1 mg/mL, 10 mg of BCP was dissolved in 10 mL 0.01 M HCl and stirred for 30-60 min. Hereafter, the solution was filtered using a 0.2 µm Nylon filter, to remove impurities. Slowly, the pH was increased from 2 to 6, by adding 1M NaOH, from there the pH was increased to 8-9, by adding 0.1 M NaOH. After three days of stirring, the Psomes were filtered with a 0.8 µm Nylon filter and crosslinked using Omnicure s2000, for 90 seconds per 2 mL polymersome solution. After crosslinking, the size, polydispersity (PDI) and ζ-potential of the Psomes were checked using dynamic light scattering (DLS) on the zeta-sizer.

For preparation of MMPsomes, two solutions were prepared; 1.0 mg/mL Psome in PBS solution at pH 6 and a 0.4 mg/mL MMP-1 in PBS solution at pH 6. These solutions were mix in a 1:1 ratio and stirred overnight. Size and ζ-potential after decoration was performed to prove decoration. Hereafter, purification was performed by dialysis using a 1000 kDa MWCO membrane against 1 M PBS dialysate change 3 times a day.

3.2 Materials in vitro studies

Psome (1mg/mL); MMP-1 (collagenase type I, prepared from Cl. Histolyticum, Sigma-Aldrich, C0130-100mg, CAS nr 9001-12-1); sterile PBS; HCl 5M (ThermoFisher); 0.2 µm Nylon filters for sterilization; 1000 kDa MWCO membrane (Spectra/Por® Membrane, Biotech CE Tubing). LX-2 cells Friedman (Mount Sinai Hospital, New York, NY, USA)*; Dulbecco's modified Eagle's medium (DMEM) (Lonza); fetal bovine serum (FBS) (Sigma-Aldrich); L-glutamine (Lonza) (Basel, CH); penicillin/streptomycin (pen/strep) (50U/ml Penicillin and 50µg/ml streptomycin, Sigma, St. Louis, MO, USA); Dulbecco's phosphate buffered saline (DPBS); TGF-β (Roche, Mannheim, Germany). 10x AB; starvation medium; 96 black bottom well plate; Victor 3 microplate reader equipped with Wallac 1420 software. GenElute™ Mammalian Total RNA Miniprep Kit (Sigma Aldrich); Nanodrop ND-1000 (Wilmington, DE, USA); UltraPure™ Distilled Water*

(Invitrogen by ThermoFisher Scientific); iScript™ cDNA Synthesis Kit (Bio-Rad Laboratories, Inc.) (Hercules, CA, USA); SensiMix™ SYBR & Fluorescein Mix (Bioline Reagents) (London, UK); Bio-Rad CXF-384™ Real-Time System. Blue loading buffer (BLB); dithiotheitol (DTT) (Cell Signaling Technology, Leiden, the Netherlands); dry bath FB 15101 (Thermo Fisher Scientific); XCell SureLock Mini-Cell Electrophoresis System (Thermo Fisher Scientific); 10% Tris-glycine gels (Life Technologies), Tris-Glycine SDS buffer (Thermo Fisher Scientific); GE Healthcare EPS 301 Electrophoresis Power Supply (Thermo Fisher Scientific); Whatman papers (Thermo Fisher Scientific); PCDF Western Blotting Membranes (Sigma); Tresfer Buffer (Bio-Rad); Monoclonal mouse anti-α-SMA (Sigma); Polyclonal goat anti-collagen I (Southern Biotech); Monoclonal mouse anti-β-actin (Sigma); Polyclonal rabbit anti-mouse IgG (DAKO); Polyclonal goat anti-mouse IgG (DAKO); Polyclonal rabbit anti-goat IgG (DAKO); Albumin Bovine Serum (Life Scientific); Pierce® ECL Plus Western Blotting Substrate (Thermo Fisher Scientific); FluorChem M Imaging System (ProteinSimple, Alpha Innotech, San Leandro, CA); NIH ImageJ software (NIH, Bethedesa, MD); Stripping Buffer (Thermo Fisher Scientific). Collagen G1 (5mg/ml, Matrix biosciences, Mörlenbach, Germany); 10x M199 medium; 1N NaOH (Sigma). Sterile scratching lid. Tissue-Tek optimum-cutting temperature (O.C.T.) embedding medium (Sakura Finetek, Torrance, CA, USA); Leica CM 3050 cryostat (Leica Microsystems, Nussloch, (Germany); Hamamatsu NanoZoomer Digital slide scanner 2.0HT; NanoZoomer Digital Pathology (NDP2.0) viewer software (Hamamatsu Photonics).

3.3 Psome and MMPsome transportation and fabrication

The used Psomes are fabricated in Dresden at IPF by Silvia Moreno, according to the protocol previously mentioned in paragraph 3.1.2. Storage of Psomes is at -20°C either frozen or freeze dried, therefore, transportation was done on dry ice. Freeze dried and frozen Psomes were rehydrated and defrosted, respectively, at the University of Twente and evaluated using the Zetasizer. The results from the frozen Psomes were more consistent and desirable. For this reason, the Psomes used in this study were all frozen Psomes.

For development of MMPsomes. Frozen Psomes were defrosted at room temperature and stirred for at least 2h under dark conditions. Afterwards, pH was adjusted to 6 using sterile 0.1M HCl and they were checked on size and charge using the zeta-sizer. Alongside, MMP-1 was dissolved in sterile PBS pH 6. Psome (1 mg/mL) and MMP-1 (0.4 mg/mL) were mixed in a 1:1 ratio and stirred overnight under dark conditions. Next day, the samples were dialyzed for 72h using a 1000 kDa MWCO against 2L PBS pH 7.4. After dialysis the samples were stored at 4°C up to seven days till further use.

3.4 General cell culturing protocol

LX-2 human HSC cell line was used, provided by Prof. Scott Friedman (Mount Sinai Hospital, New York, NY, USA). The cells were cultured in Dulbecco's modified Eagle's medium (DMEM) containing 10% fetal bovine serum (FBS), 1% L-glutamine and 1% penicillin/streptomycin (pen/strep) (Sigma Aldrich), hereafter called 10% FBS medium, and stored in the incubator at 37°C and 5% CO_2. The cells were passaged twice a week, when they reached 100% confluency. When passaging or plating, the cells were first washed with Dulbecco's phosphate buffered saline (DPBS) and then incubated with trypsin for a couple of minutes before passaging.

Experiments were performed in 12 well bottom treated culture well plates. In a 12 well plate cells were plated with $1*10^5$ cells per mL, 1 mL per well. Using 10% FBS medium and incubated overnight or at least 4h. Next day, the cells were starved using DMEM, 0% FBS, 1% L-glutamine, 1% pen/strep, hereafter called starvation medium, and again incubated overnight.

Before cell treatment, MMP-1, Psome and MMPsome solutions were diluted using starvation medium. Final concentrations of MMP-1 were 0.25, 0.5, 1.0, 2.5 and 5.0 µg/mL, hereafter called MMP (0.25), MMP (0.5) etc. These concentrations are complementary to free Psome concentrations of 2.83, 4.17, 8.33, 20.83 and 41.67 µg/mL, hereafter called Psome (0.25), Psome (0.5) etc. Consequently, concentration of MMPsome were 0.25, 0.5, 1.0, 2.5 and 5.0 µg MMP-1/mL, 2.83, 4.17, 8.33, 20.83 and 41.67 µg Psome/mL respectively, hereafter called MMPsome (0.25), MMPsome (0.5) etc. Thereafter the cells were treated with different concentrations of free MMP-1, free Psome or MMPsome and/or activated with TGF-β (final concentration of 5 ng/mL) to reach the aforementioned concentrations and incubated for 24 (viability, gene expression, migration assay) or 48h (protein expression, migration assay). This protocol is visualized in **Figure 4**.

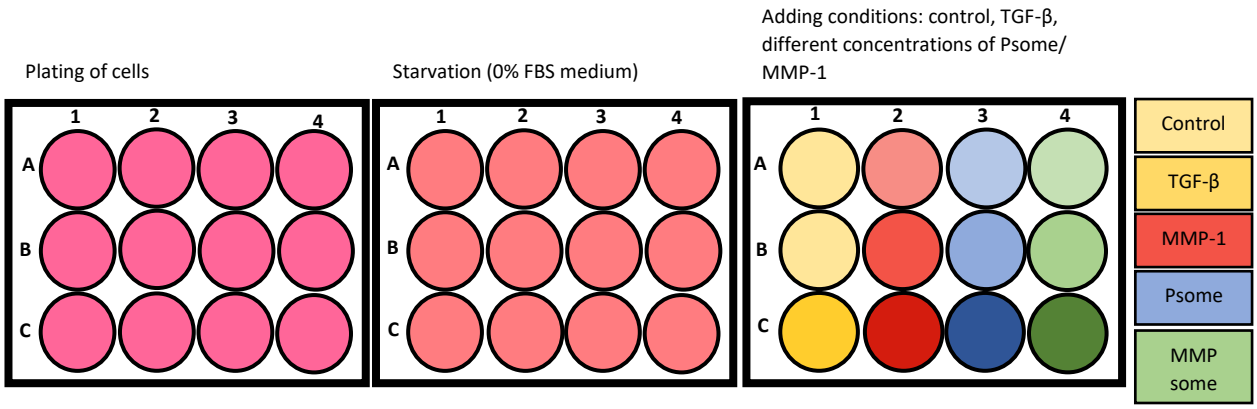

Figure 4. *Overview of plating, starving and activation. Cells were plated with a density of 10^5 per well (1 mL) and starved 4-24 h later. Activation was performed 24 h after starvation by first adding 500 µL of either normal starvation medium or MMP-1, Psome or MMPsome containing medium. Followed by 500 µL of either normal or TGF-β containing medium. Final concentrations were 0.25, 0.5, 1.0, 2.5 or 5.0 µg/mL MMP-1 with complementary concentration of Psome and 5 ng/mL TGF-β.*

3.5 Viability assay

The viability of Psomes and MMPsomes were tested using an Alamar Blue Assay (ABA). The cells were plated, starved and activated as mentioned previously. After 24h of incubation the medium was removed and the cells were washed once using 500 µL PBS. Simultaneously, 1x Alamar blue (AB) medium was prepared by dissolving 10x AB in starvation medium in a 1:10 ratio, under dark conditions. After washing, the cells were incubated with 500 µL 1x AB medium for 4h at the back of the incubator. After incubation, three time 150 µL medium of each well was collected in a 96 black bottom well plate and the absorbance of the medium was measured using the Victor 3 microplate reader. The data was processed using Wallac 1420 software. The mean values of three measurements were used and compared to the TGF-β activated condition, which is set to 100% viability.

3.6 qPCR

Gene expression was measured using quantitative polymerase chain reaction (qPCR). The cells were plated, starved and activated as mentioned previously. After 24h of incubation the medium was removed and the cells were washed once using 500 µL PBS. Then, RNA was obtained by lysis and isolation according to the manufacturer's instructions described in the GenElute™ Mammalian Total RNA Miniprep Kit retrieved from Sigma Aldrich. If not used directly, the RNA was stored at -80°C. After isolation the RNA concentration and the purity were measured with Nanodrop. Afterwards, the RNA was diluted with distilled water to reach equal concentration in every condition and cDNA was synthesized using the

iScript™ cDNA Synthesis Kit, according to the manufacturer's description. After synthesis, the cDNA was again diluted to 10 ng/µL using distilled water. If not used directly, the cDNA was stored at -20°C. Preparation for qPCR consisted of preparing primer mixes, containing 1.9 µL distilled water, 0.05 µL forward primer and 0.05 µL reverse primer per sample. 4 µL SYBR reagent was added mixed directly before use. All samples were measured in duplicate. For measuring a 384 wells plate was used. Firstly, 2 µL of cDNA was added to the wells plate, in columns. Then, after adding and mixing the SYBR agent, 6 µL of primer mix was added, in rows. Example of a wells plate is shown in **Figure 5**. The plate was sealed with a transparent lid and the wells plate was centrifuged for 1 min at 4000 rpm. Lastly the qPCR was done according to a pre-configurated protocol, using the Bio-Rad CXF-384™ Real-Time System.

For analysis of qPCR results al genes of interest (collagen-1, collagen-3, α-SMA, TIMP-1 and MMP-1) are normalized to two different housekeeping genes (GAPDH and 18s-RNA, also called RPS-18), primers for the genes are specified in Appendix C, **Table 3**. After normalization the fold induction compared to the activated state (TGF-β) is calculated.

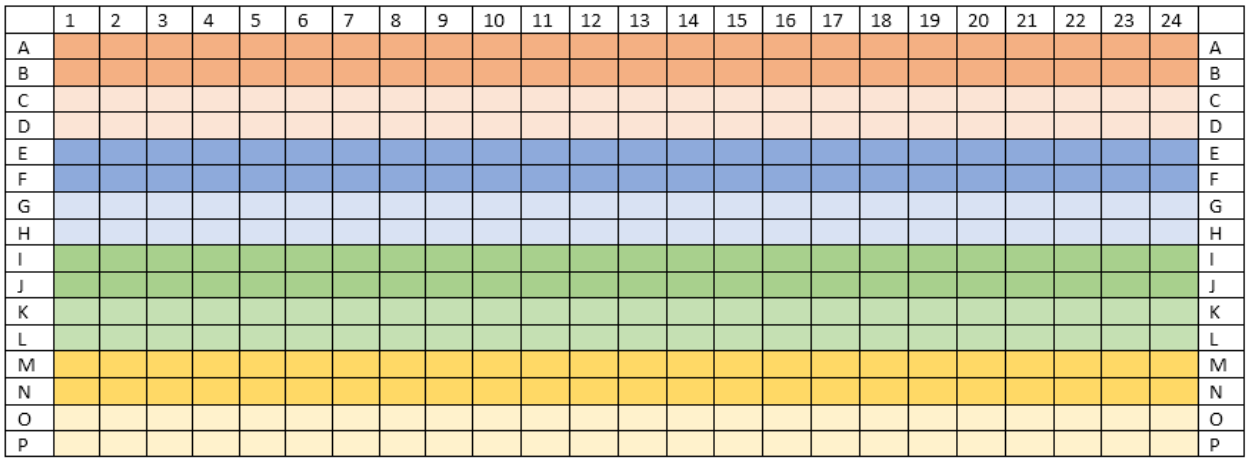

Samples	
1. Control-1	13. Control-1
2. Control-2	14. Control-2
3. TGF-β	15. TGF-β
4. MMP-1 (0.25)	16. MMP-1 (0.25)
5. MMP-1 (0.5)	17. MMP-1 (0.5)
6. MMP-1 (1.0)	18. MMP-1 (1.0)
7. Psome (0.25)	19. Psome (0.25)
8. Psome (0.5)	20. Psome (0.5)
9. Psome (1.0)	21. Psome (1.0)
10. MMPsome (0.25)	22. MMPsome (0.25)
11. MMPsome (0.5)	23. MMPsome (0.5)
12. MMPsome (1.0)	24. MMPsome (1.0)

Genes (1-24)	
A. Coll 1α1	B. Coll 1α1
C. Coll 3α1	D. Coll 3α1
E. αSMA	F. αSMA
G. TIMP-1	H. TIMP-1
I. MMP-1	J. MMP-1
K. GAPDH	L. GAPDH
M. 18-s RNA	N. 18-s RNA
O.	P.

Figure 5. *Overview of 384 well PCR plate. Samples are added in the columns according to the table down left, genes are added in the rows in duplicate according to the table down right.*

3.7 Western Blot

Protein expression is measured using western blot (WB). First, the cells were plated, starved and activated as mentioned previously. After 48h of incubation the medium was removed and the cells were washed once using 500 µL PBS. The cells were lysed using a mixture of sterile water with blue loading buffer and DTT. This was stored at -80°C. The lysate was collected in eppendorfs and heated at 96°C in the dry bath

for 5-10 min. The XCell SureLock Mini-Cell Electrophoresis System was prepared according to the manufacturer's instructions using Tris-Glycine SDS buffer. The samples were loaded in 10% Tris-glycine gels and the gel was run for 60-90 min using electrophoresis power supply EPS 301. After gel electrophoresis, the gel is cut in to remove the chambers and form a rectangular shape. Hereafter, the proteins were blotted on a polyvinylidene fluoride (PVDF) membrane. This was done using western blot sandwiching. The sandwich consisted of a Whatman filter, with on top the PVDF membrane. Hereon, the gel was placed with the proteins facing the membrane, the sandwich was finished with another Whatman filter. Whatman filter, the membrane and the gel are pre wetted in blotting solution. Blotting was performed for 1 h. After blotting the Whatman filters and gel were removed. The PVDF membrane was cut into two pieces, to create a lower part for proteins with a lower size (α-SMA (48 kDa) and β-actin (40 kDa)) and a greater size (coll-I (120 kDa)). Both membranes were blocked for 1 h at room temperature using albumin bovine serum (BSA) blocking buffer. After blocking, the membranes were incubated with the first antibody (AB) α-SMA (1:500) and coll-1 (1:600) overnight at 4°C. After this the membranes were washed and incubated with the second AB (1:1000) and for 1h. At last, after washing again, the bands on the membranes were developed with Pierce® ECL Plus Western Blotting Substrate and pictured with FluorChem M Imaging System. The intensity of the bands was analyzed using ImageJ and standardized to the intensity of the activated TGF-β sample. Since α-SMA and β-actin are localized on the same membrane, development of β-actin was performed after development of α-SMA. When α-SMA was pictured, the membrane was stripped using stripping buffer and blocked using blocking buffer. Hereafter, β-actin (1:5000) could be developed according to the aforementioned protocol, accept for the first AB which was incubated for 1h at room temperature.

3.8 Contractility assay

Contractility assay was performed to measure the *in vitro* stiffness. For the contractility assay a collagen suspension consisting of collagen, sterile water, M199 medium and NaOH was prepared. Cells were mixed with this suspension directly after preparation and the cell-gel-suspension was set to polymerize for 1h at 37°C. After polymerization, normal starvation medium, TGF-β medium or TGF-β medium with a certain MMP-1 concentration (0.5, 1.0, 2.5 or 5.0 µg/mL) was added and incubated. Pictures were made after 24 and 48 h.

Due to observations (discussed in results and discussion section) an alternative set-up, based on the article of Kobayashi et al. was used (38). Firstly, the cells were plated and starved in a 6 wells-plate and incubated for 4 h to attach. After four hours, the cells were starved using 0% medium and incubated overnight. The next day, the cells were stimulated using TGF-β and MMP-1, except for the control, and incubated for 24 hours. After 24h, the cells were trypsonized, spun down and the conditioned medium was removed. The cells were mixed with freshly prepared collagen suspension. After polymerization, non-conditioned 0% medium was added and photos were made after 24 and 48h.

3.9 Scratching assay

The cells were plated and starved in a 12-wells plate according to previously mentioned protocol. After overnight incubation with starvation medium, a scratch was made using a 200 µL pipet tip. This scratch was directed by a special vertical scratching lid that fit the 12-wells plate. Perpendicular to the scratch, in the middle of the wells plate, a line was drawn with a waterproof black marker. Directly after scratching the cells were washed with 500µL PBS and activated with TGF-β and/or treated with MMP-1, Psome and MMPsome with different concentrations (0.25, 0.5 or 1.0 µg MMP-1/mL). Pictures were made after 0h, 24h and 48h. To ensure all the pictures were made of the same part of the scratch, the picture was either

made directly above or directly under the black marker line, perpendicular to the scratch. Migration was calculated using ImageJ.

Besides the manual picturing, we had the opportunity to perform a scratching assay with the CytoSMART™ Omni. This live-cell imager is equipped with software that can identify a scratch and can accurately measure the surface of the scratch. The work protocol was similar, except the pictures are made inside the incubator and analysis was done by the software.

3.10 In and ex vivo mouse model study

To study the *in* and *ex vivo* effect of MMP-1, Psome and MMPsome, a fibrotic mouse model was used. The mice used in this study were C57BL6, also called C57 Black 6, a widely used breed (39). Only male mice were used, since female hormones can affect the fibrosis progression, which causes variations. After arrival, the mice were randomly distributed in a control group, CCl_4 group, MMP-1 group and MMPsome group and normally fed with dry food and water for one week. On day 1, mice were intraperitoneally injected with 1 mL/kg CCl4 in olive oil (1 CCl_4 : 5 olive oil), single dose injection. On day 3, they received either MMP/MMPsome single dose treatment. 170 µL free or decorated MMP (60 µL/mL) was slowly intravenously injected, to minimize aggregation. On day 4, mice were sacrificed by cervical dislocation and the liver, lungs, spleen, kidneys and heart were harvested for further analysis. Visualization of the protocol is pictured in **Figure 6**. Analyzing methods comprised of liver weight analysis, immunohistochemistry staining and PCR.

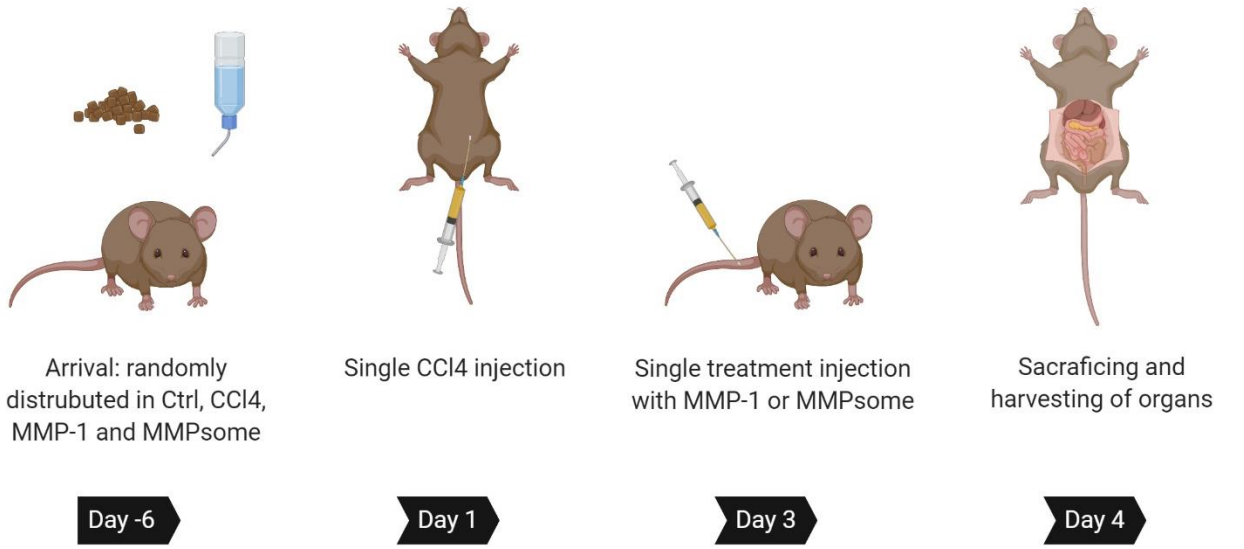

Figure 6. *Overview of the in vivo experiment. Mice were randomly distributed upon arrival and fed normally. On day 1, mice were injected with CCl4 (1 ml/kg). On day 3, mice were treated with MMP or MMPsome (10.2 µg). On day 4, the mice were sacrificed and the organs were harvested.*

3.10.1 Ex vivo study

Four livers of CCl_4 treated mice were used for *ex vivo* studies. Per liver four small rectangular block from 1x1x1 mm were cut and incubated with either M199 serum, MMP-1 (50 µg/mL) M199 serum, Psome (417 µg/mL, complementary to 50 µg/mL MMP-1) M199 serum or MMPsome (50 µg/mL MMP-1, 417 µg/mL Psome) M199 serum, for 4h at 37 °C under dark conditions. Afterwards, samples were transferred to Tissue Tek medium and snap frozen in 2-methyl butane on dry ice.

3.10.2 Staining

The *in vivo* samples were also transferred to Tissue Tek medium and snap frozen in 2-methyl butane on dry ice after harvesting. After snap freezing all samples (*in* and *ex vivo*) were cut in 7 µm sections using the cryostat. All sections were scanned using the Nanozoomer for histological analysis. High resolution scans were viewed using the viewer software and analyzed using ImageJ. Sections were stored at -20°C.

Before use, the sections were dried under a hairdryer for 30 min. After drying, the sections were fixed with acetone for 20 min and then dried again for 15 min. The sections were circled using a hydrophobic DAKO pen and rehydrated with PBS for 5 min. The first antibody is diluted (collagen 1:100, F4-80 1:100) and incubated overnight. The next day the sections were rinsed three time with PBS, 5 min each and incubated with hydrogen peroxide dissolved in methanol for 30 min. Afterwards they were rinsed once with MilliQ and washed three times with PBS, 5 min each. The second AB was diluted (1:100) in 5% mouse serum and incubated for 1 h. Again, the sections were washed with PBS three times, 5 min each and then incubated with the tertiary AB and incubated for 1 h. Afterwards they were washed three times with PBS, 5 min each and stained for 20 min with AEC according to the manufacturer's instructions. They were washed once with MilliQ and counterstained with hematoxylin for 2 min. Lastly, they were washed with tap water for at least 5 min and mounted using aquatex mounting medium.

Chapter 4 Results

Here, in this chapter, all the results will be shown and objectively described.

4.1 Characterization of MMPsomes

To evaluate the decoration of MMP-1 to the Psome, the alterations in size and charge using the ζ-sizer were measured. Furthermore, the decoration efficiency was measured using RhB labeled MMP-1. Lastly, the loss of activity due to decoration was determined using an activity assay.

4.1.1 Zeta-sizer results

Table 1. *Results retrieved from Zeta-sizer. Size of Psome decreases with increasing pH. Size increases after decoration, as does the PDI. ζ-potential decreases with increased pH, as does after decoration.*

Sample	Size (nm)	PDI	ζ-potential
Psome pH 6	158,0	0,201	19,0
Psome pH 8	107,5	0,227	7,23
Psome + MMP-1 pH 6	180,5	0,334	7,70
Psome + MMP-1 pH 8	145,8	0,277	-3,98

Results are demonstrated in **Table 1**. In collapsed state (pH 8) the Psome has decreased in size, compared to the swollen state. After decoration, the size is also increased, compared to undecorated Psome. Furthermore, the ζ-potential is lower at more basic solutions, concluding from the difference between pH 6 and 8. Lastly the ζ-potential is also lower when MMP-1 is decorated at the outer surface of the Psome.

4.1.2 Decoration efficiency

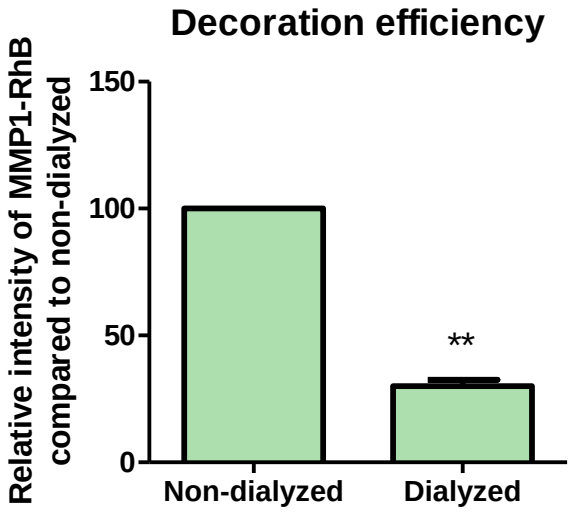

Figure 7. *Decoration efficiency measured using RhB labelled MMP-1 before and after purification by dialysis using 1000 kDa MWCO membrane against 1x PBS for 72 h, dialysate refreshed 3 times a day. Significance calculated using an unpaired t-test CI 95%, p<0.01.*

The intensity of RhB, and thereby the number of MMP-1 enzymes, after dialysis is one third of the intensity before dialysis. Significance is measured using an unpaired t-test with confidence interval of 95%, p<0.01. Data demonstrated in **Figure 7**.

4.1.3 MMP-1 activity after decoration

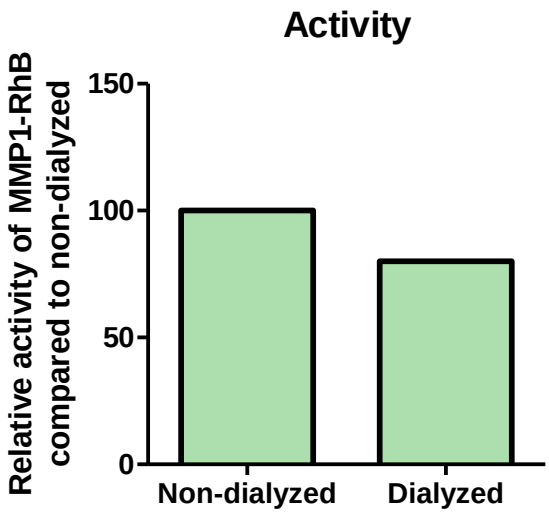

Figure 8. *Activity test before and after purification by dialysis, using a 1000 kDa MWCO membrane against 1x PBS for 72 h, dialysate refreshed 3 times a day. Activity is decreased by 80%.*

The activity of MMP-1 after dialysis is 80%, compared to the activity before dialysis, shown in **Figure 8**. The activity is measured using the collagenase activity colorimetric assay kit (Sigma-Aldrich). The absorbance of the substrate is decrease by the digestion of FALGPA by MMP-1. The slope of this decrease is activity.

4.2 Viability assay

Viability was measured using ABA. Results of this experiment are displayed in **Figure 9**. '*' indicates significant difference compared to TGF-β, '#' indicates significant difference compared to ctrl.

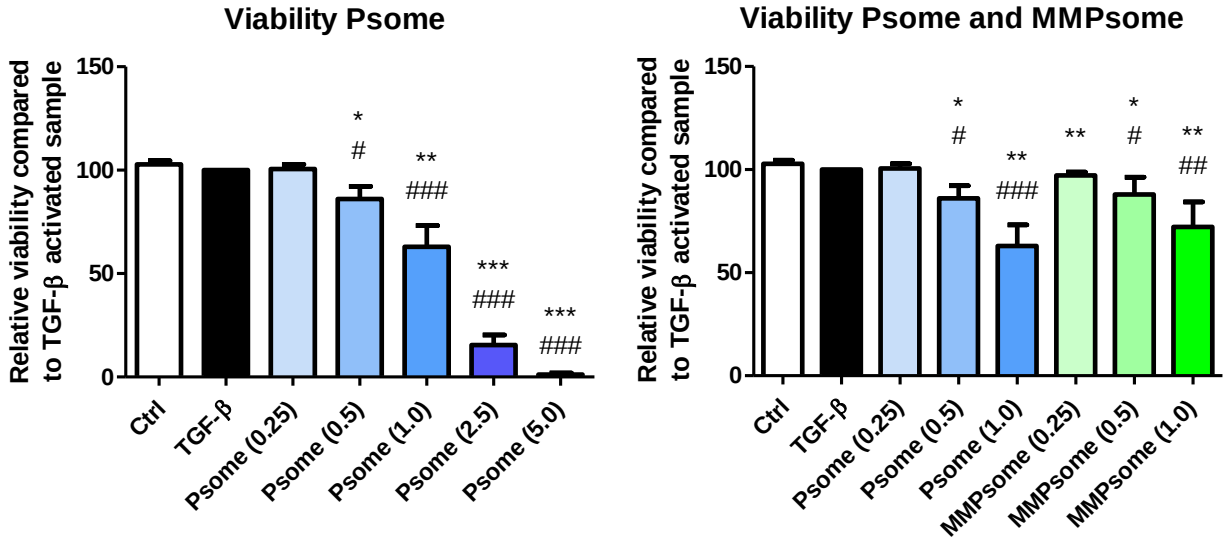

Figure 9. *Viability results from ABA. Viability of Psome ctrl 103%, TGF-β 100%, Psome (0.25) 101%, Psome (0.5) 86%, Psome (1.0) 63%, Psome (2.5) 15% and Psome (5.0) 1%, MMPsome (0.25) 97%, MMPsome (0.5) 88% and MMPsome (1.0) 72%. Significance is calculated with an unpaired t-test CI 95%, * p<0.05, ** p<0.01, *** p<0.001, # p<0.05, ## p<0.01, ### p<0.001*

Looking at "Viability Psome", no significant difference between ctrl, TGF-β and Psome (0.25) is found. The viability of cells and the concentration of Psome are inversely proportional; if the concentration of Psome increases, the viability decreases. At a concentration of Psome (2.5) and (5.0), the Psome is non-viable (<20%) and therefore not used in further experiments.

Viability of MMPsome was also tested. There is a significant decrease of viability between TGF-β and all MMPsome samples, however, all samples have a viability above 70%.

4.3 qPCR

Different sets of genes were tested We will firstly analyze fibrotic markers coll-1, coll-3 and α-SMA, where after we continue to MMP-1 and TIMP-1 expression.

4.3.1 Fibrotic markers

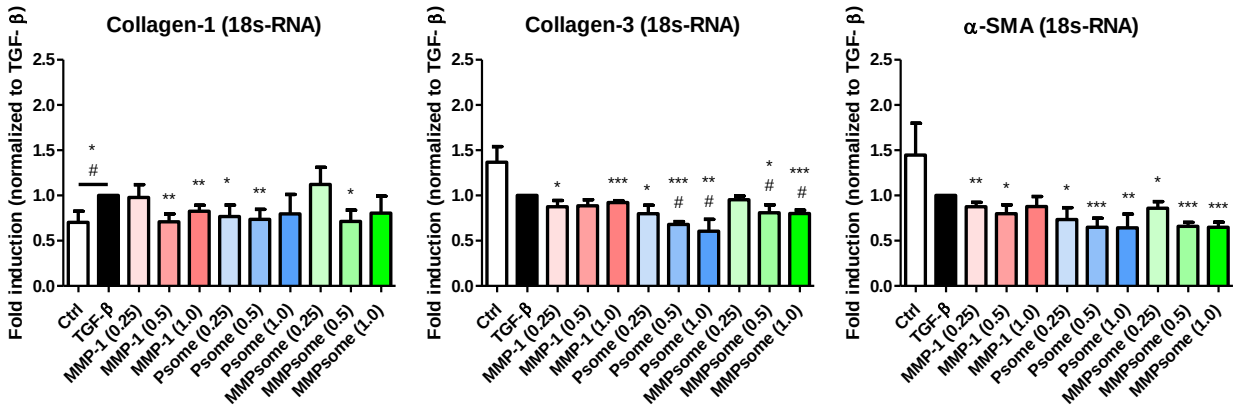

***Figure 10**. Expression of different fibrotic genes; coll-1, coll-3 and α-SMA. The stars '*' and hashtags '#' indicate significant difference compared to TGF-β and ctrl, respectively. Significance was determined with the unpaired t-test, CI 95%, */# p<0.05, **/## p<0.01, ***/### p<0.001.*

With qPCR fibrotic genes coll-1, coll-3 and α-SMA were tested, results displayed in **Figure 10**. In coll-1 a significant increase of coll-1 is visible in the fibrotic TGF-β sample, compared to the ctrl. Furthermore, in this graph, a significant decrease of different conditions is indicated. For coll-3 there is no significant difference between ctrl and TGF-β. However, there is a significant decrease of coll-3 in almost all activated samples compared to the TGF-β activated fibrotic model. The same is visible in α-SMA, no significant difference between ctrl and TGF-β, however there is a significant decrease in most treated samples.

4.3.2 MMP-1 and TMP-1 expression

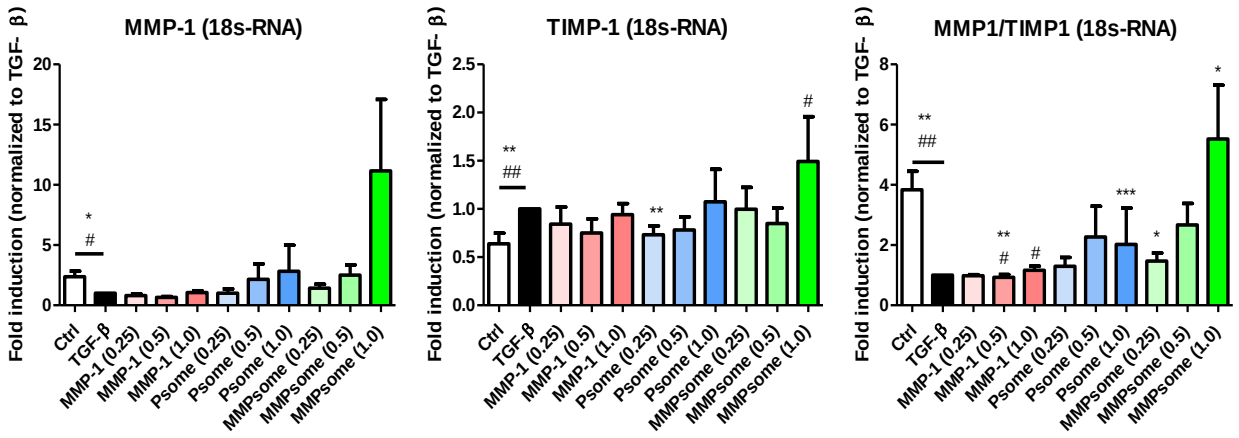

Figure 11. *The expression of MMP-1, its inhibiter TIMP-1 and the relative ratio of both genes MMP1/TIMP1. The stars '*' and hashtags '#' indicate significant difference compared to TGF-β and ctrl, respectively. Significance was determined with the unpaired t-test, CI 95%, */# p<0.05, **/## p<0.01, ***/### p<0.001.*

Significant difference between MMP-1, TIMP-1 and MMP1/TIMP1 expression is visible in **Figure 11**. In MMP-1 expression there is a dose dependent response of all treatments, however non-significant. TIMP-1 does not show dose dependent responses, except for the Psome treatments. In the MMP-1 treated sample, the expression is higher, compared to ctrl, but lower compared to TGF-β, however non-significant. The Psome treated samples show a significant decrease in the lowest dose. The MMPsome treated samples, show no significant difference compared to the TGF-β activated sample, however, the highest dose does increase the expression, which is significant compared to the ctrl. Lastly, the ratio of MMP1-TIMP1 expression is calculated and shows significant difference between ctrl and TGF-β, also there is significant difference between the highest two MMP-1 treated samples. Furthermore, there is a significant increase in the Psome (1.0) treated sample compared to the TGF-β. Lastly, also the MMP-some treated samples show an increase, of which two are significant.

4.4 Western blot

Expression of two different fibrotic markers are visualized in **Figure 12**. α-SMA shows now significant difference between ctrl and TGF-β. The only significance is the decrease of expression in the Psome (1.0) treatment. MMP-1 shows a dose dependent increase, however non-significant, while Psome and MMPsome show a dose dependent decrease. Coll-1 shows significant increase of expression upon TGF-β activation, with p<0.001. All treatments show a dose dependent, significant decrease of coll-1 expression. MMP-1 shows a significant increase compared to the ctrl, without a significant difference compared to the TGF-β sample. Psome treated samples show a dose dependent response with a significant decrease in the highest concentration. MMPsome also shows a dose dependent response, with significant decrease in the MMPsome (0.5) and (1.0).

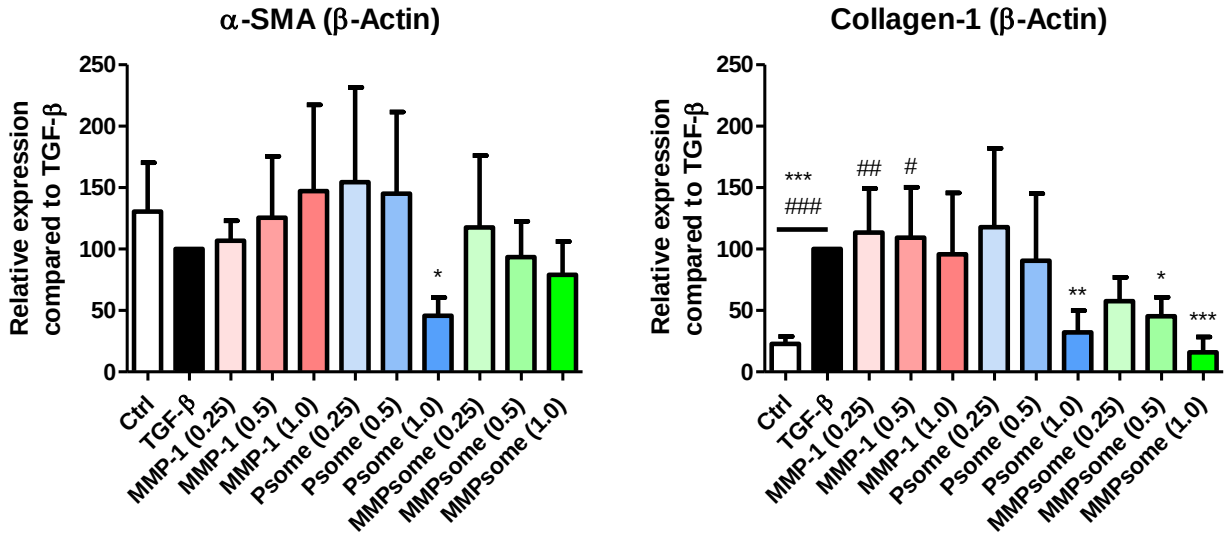

Figure 12. *Protein expression of α-SMA and coll-1 measured with WB and normalized to β-actin. The stars '*' and hashtags '#' indicate significant difference compared to TGF-β and ctrl, respectively. Significance was determined with the unpaired t-test, CI 95%, */# p<0.05, **/## p<0.01, ***/### p<0.001.*

4.5 contractility assay

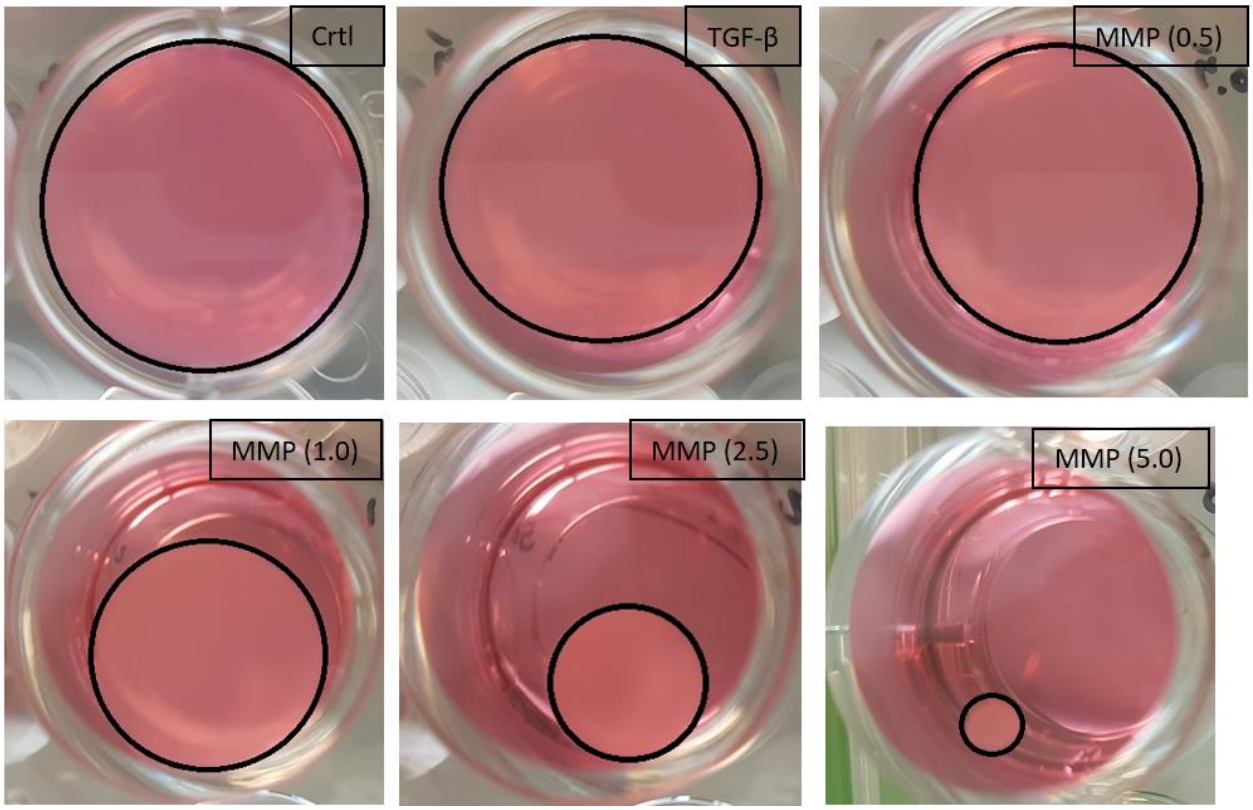

Figure 13. *Contractility assay, pictures of collagen matrix after 48h. The black circle markers the edge of the collagen matrix. The decrease of surface can be measured compared to the surface of the well.*

As displayed in **Figure 13**, the surface area of ctrl is not decreased compared to the well border. In contrast, the surface area of the TGF-β stimulated sample is decreased compared the well border. Moreover, the MMP-1 treated sample show a dose dependent decrease of surface area, compared to the well border.

4.6 Wound healing assay

4.6.1 Manual WHA

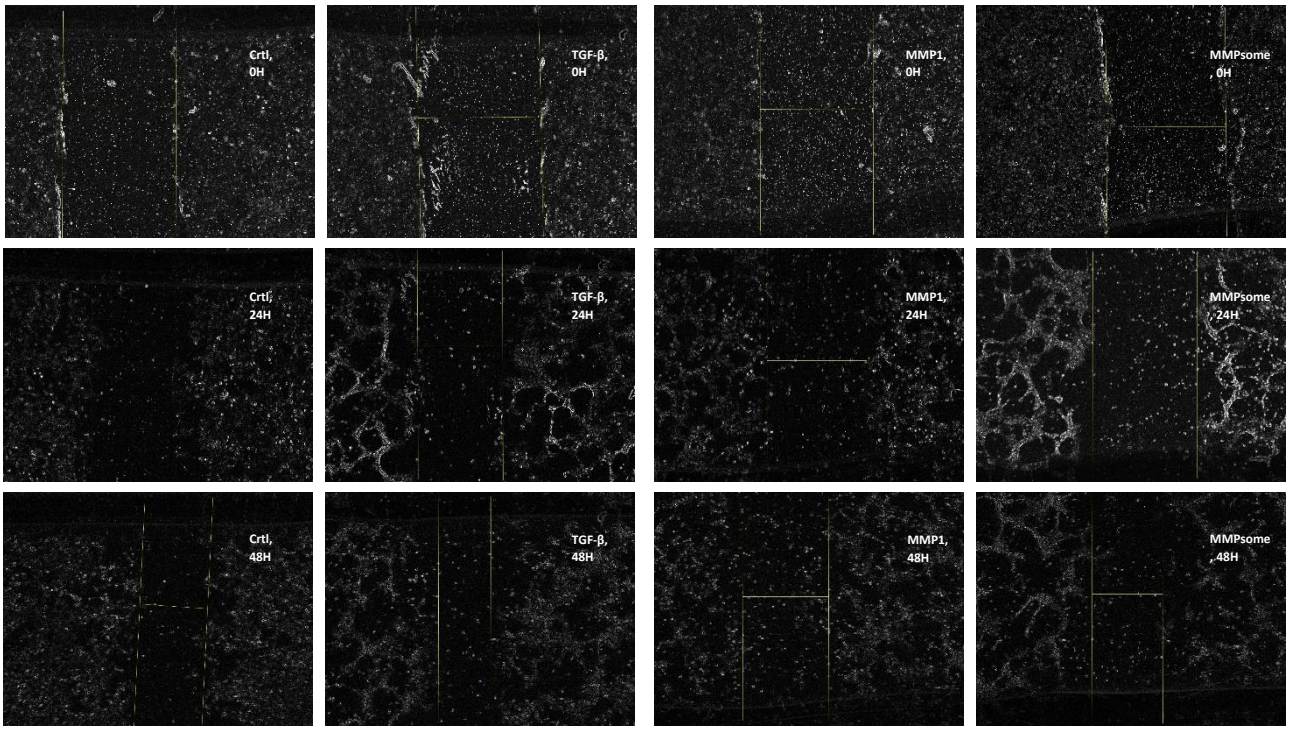

Figure 14. *Overview of raw data. Two parallel vertical lines are drawn at the border of the scratch. Perpendicular a horizontal line is drawn and measured, indication the width of the scratch. Data shown of 4 samples: ctrl, TGF-β, MMP-1 (1.0) and MMPsome (1.0) at 9, 24 and 48 h.*

Concluding from **Figure 14** it can be stated that there is a decrease in width visible in all samples. Quantification of this decrease is visualized in **Figure 15**.

After 24h, a dose dependent response is visible in MMP-1 and MMPsome. The wound healing is inversely proportional to the treatment dose. MMP-1 has a significant decrease of healing in the highest dose compared to TGF-β and ctrl. Also, MMPsome has significant decrease after 24h, in the two highest concentrations. MMPsome (0.5) has significant decrease compared to TGF-β, MMPsome (1.0) too, besides a significant decrease compared to the ctrl. The Psome also seem to have a dose dependent response, however higher concentrations have higher wound healing. Still, only the highest concentrations have significant decrease of wound healing compared to TGF-β.

The wound healing after 48h shows a higher significant difference between ctrl and TGF-β. In MMP-1, there is only a significant decrease visible in the highest concentration, compared to TGF-β as well as the ctrl. The Psome does not show a dose dependent response. Psome (1.0) does not have an error bar since most of the samples were unable to be measured after 48h due to a high number of dead cells, that inhibited the quantification. MMPsome shows a dose dependent response with significant decrease in the highest two samples.

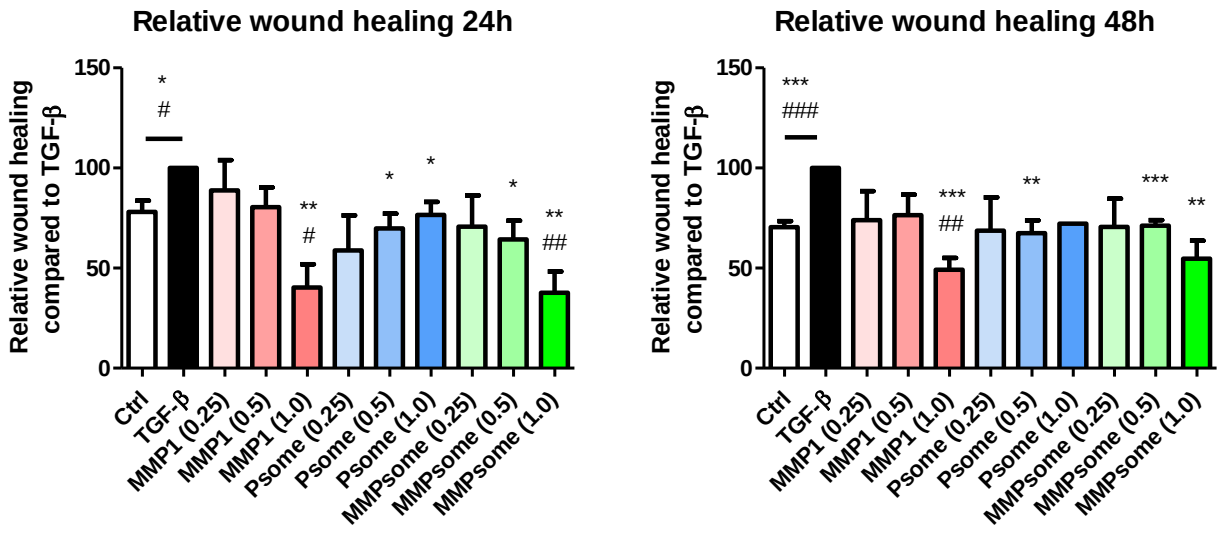

Figure 15. *Relative wound healing compared to TGF-β. The stars '*' and hashtags '#' indicate significant difference compared to TGF-β and ctrl, respectively. Significance was determined with the unpaired t-test, CI 95%, */# p<0.05, **/## p<0.01, ***/### p<0.001.*

4.6.2 WHA performed using CytoSMART™ Omni

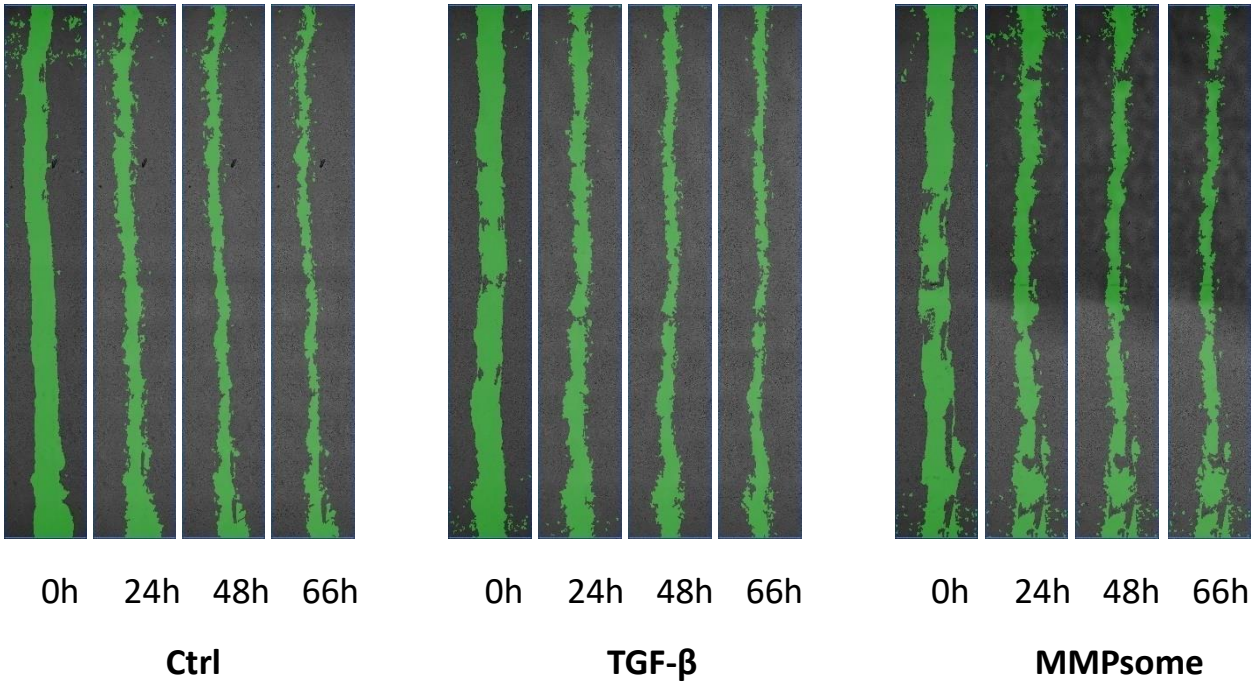

Figure 16. *Raw data of WHA performed with CytoSMARTTM Omni. Area at the middle of the well where the scratch is made is used for data analysis. The software highlighted the scratch and measured the cell-less area every 2h. Pictures after 0, 24, 48 and 66h are displayed.*

In **Figure 16** the raw data made by the software of CytoSMART™ Omni is demonstrated. The software recognizes the cell-less area as scratch and highlights it. Every 2h a picture is made and the area of the scratch is measured. This data is used to calculate the relative wound healing compared to TGF-β, this data

is displayed in **Figure 17**. It shows low difference between ctrl and TGF-β and MMP-1. Furthermore, is shows the lowest wound healing in the MMPsome treated sample.

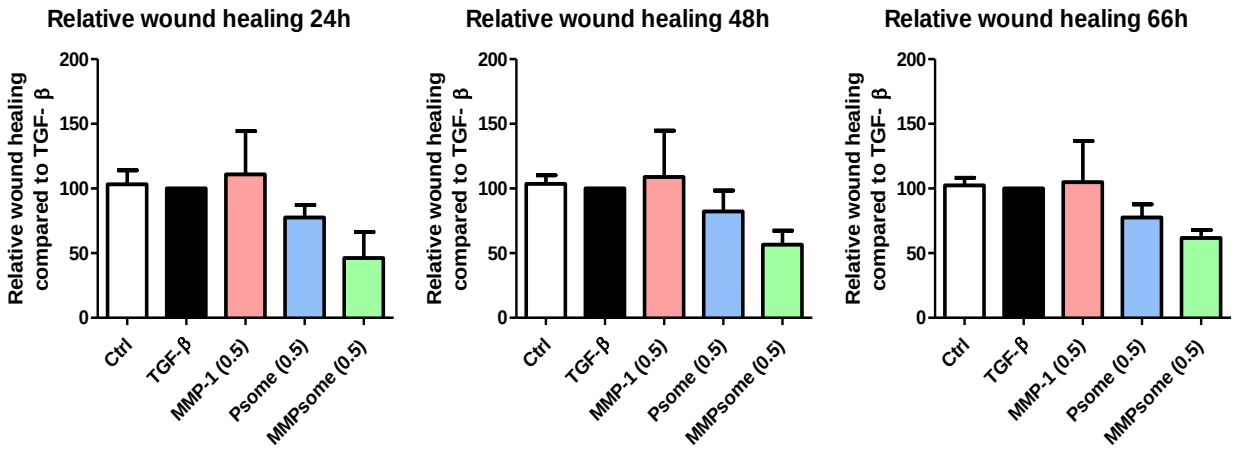

Figure 17. *Relative wound healing compared to TGF-β after 24, 48 and 66h.*

4.7 In and ex vivo mouse model study

4.7.1 Liver-to-body weight

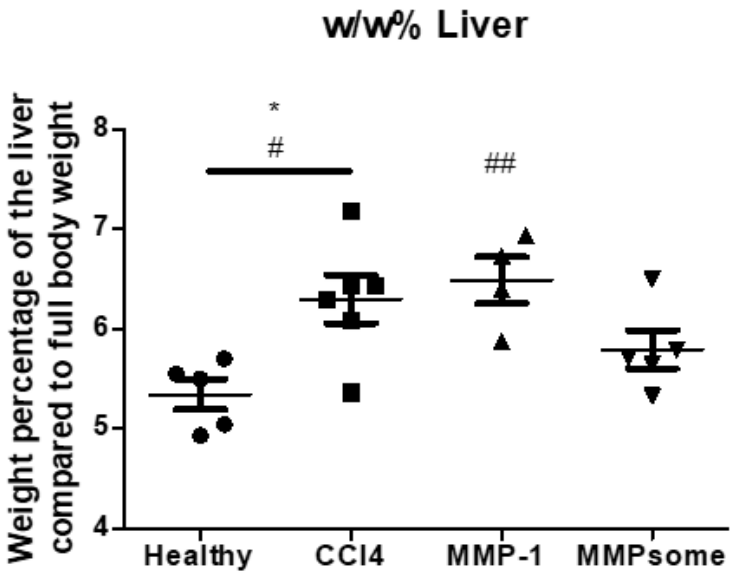

Figure 18. *The weights of the livers are displayed as a percentage of their full body weight. There is a significant increase of the w/w% of the liver of CCl4 mice, compared to the healthy control. CI 95%, p<0.05. Higher significance is present in the MMP-1 treated samples CI 95%, p<0.01. No significant difference is found in MMPsome treated samples.*

Figure 18 shows the liver-to-body weight of healthy, CCl_4 induced fibrotic mouse model, MMP-1 treated and MMPsome treated mouse group. There is a significant increase of liver-to-body weight in the CCl_4 group compared to the healthy group. This significant difference is also visible in the MMP-1 treated group. The MMPsome treated group show no significant difference with any other group.

4.7.2 ex vivo staining

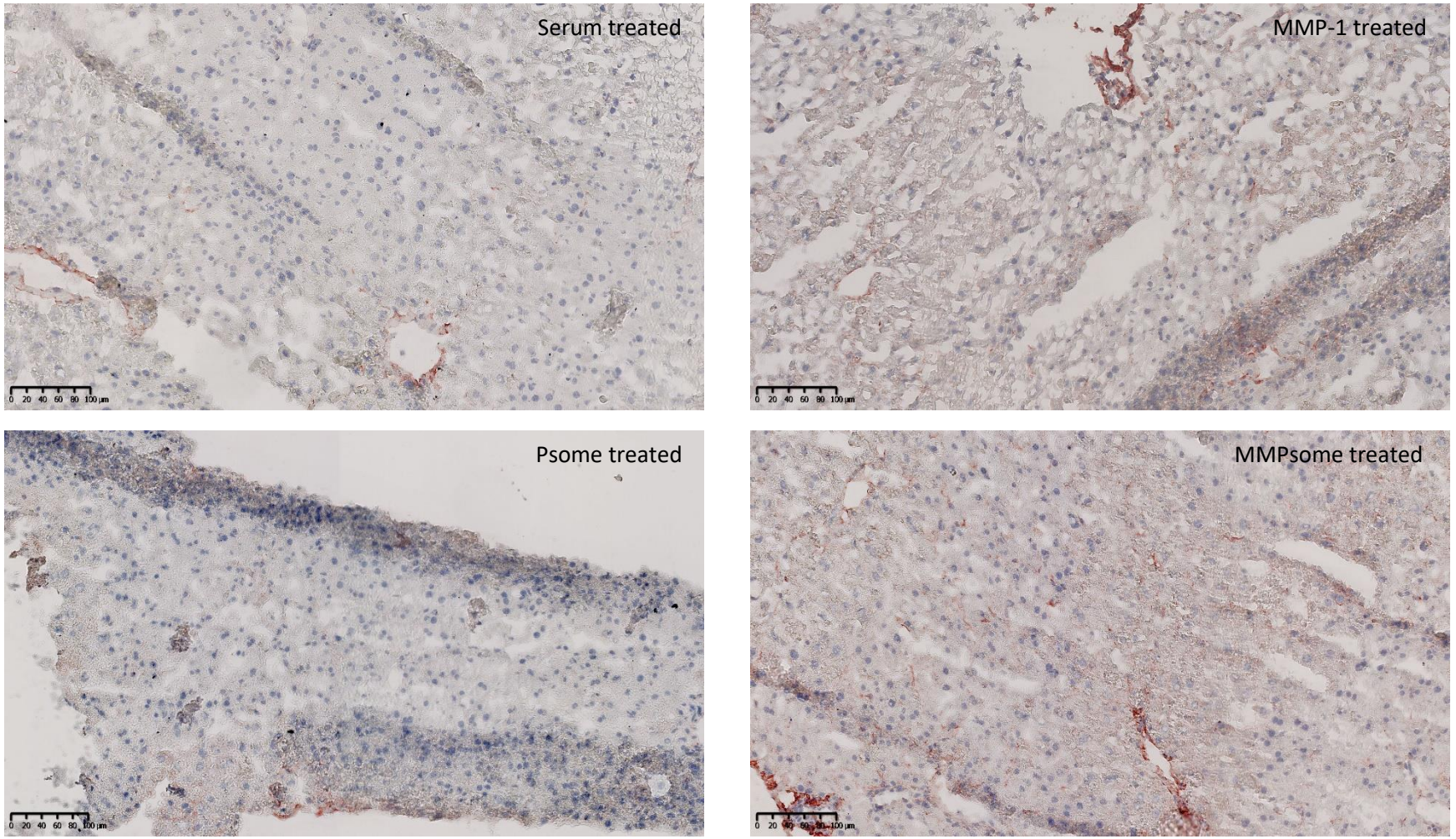

Figure 19. *Ex vivo study, coll-1 staining. Serum treated, MMP-1 treated, Psome treated and MMPsome treated samples. Ex vivo incubated for 4h. The photos are representable for the ex vivo study.*

The photos displayed in **Figure 19** are representable for the *ex vivo* study. Quantification yet has to be performed. Blue dots are the cell nuclei, red is the collagen in ECM.

Chapter 5 Discussion

In this chapter all the results of chapter 4 are elaborately discussed and explained. Furthermore, the impact of this research will be evaluated.

5.1 Characterization of MMPsomes

5.1.1 DLS

As shown in the results in **Table 1**. The size of the Psome is pH depending, from 6-8. This is due to the pH responsive block in the BCP. At low pH, 6, the DEAEMA interacts with H+ and therefore the membrane gets swollen, this increases the size. The size also depends on decoration. MMP-1 is decorated on the outer surface of the Psome and therefore increases the size of the Psome. These results show successful decoration. Furthermore, the decrease of ζ-potential is also supporting data for successful decoration. The enzyme itself is negatively loaded, decoration on the outer surface of the Psome therefore decrease the surface potential. Altogether, data retrieved from DLS prove successful decoration.

5.1.2 Decoration

To measure the decoration efficiency, MMP-1 is labelled with RhB. The intensity before and after purification is measured and demonstrated in **Figure 7**. Due to dialysis purification, the intensity measured afterwards is established only by the decorated enzyme, since all free enzyme is drained. This intensity can be compared to the intensity before purification and this is the decoration efficiency.

The intensity after dialysis is 30%, meaning that 70% of the enzyme is drained, since it was not decorated on the surface of the Psome. Therefore, we can conclude that the decoration efficiency is 30%.

5.1.3 MMP-1 activity after decoration

The decoration efficiency was successfully measured using RhB labelled enzyme. However, more important is the influence of decoration on the activity of MMP-1. For this, the activity of MMP-1 before and after decoration is measured using the collagenase activity colorimetric assay kit (Sigma-Aldrich) was used, data is displayed in **Figure 8**. Since the decoration efficiency is 30%, it is expected that the activity of MMPsome after dialysis purification is 30% of the activity before dialysis, if the Psome has no influence of the activity. However, the activity of dialyzed MMPsome is 80%, compared to non-dialyzed MMPsome. The explanation can be found in the storage prescriptions of the enzyme. According to Sigma Aldrich, it has to be stored at -20°C. However, due to fabrication of MMPsomes and dialysis, the enzyme is at room temperature for a week, before measurements. A possible explanation is that the Psome protects the MMP-1 from losing activity, while the free enzyme loses activity, due to the storage at room temperature.

5.2 Viability assay

Alamar blue is a non-toxic compound used to test the viability of the cells. The active ingredient is resazurin, a non-fluorescent blue dye that can be reduced to the pink-colored highly fluorescent resorufin (40). This is done by metabolic activity of cells. Therefore, it tests the metabolic activity of cells, not directly the viability. Beside the ABA, the cells were also checked under the microscope right before adding the Alamar blue, this showed that in the less metabolic samples, there were indeed fewer living cells. Hence, we can state that ABA is a justly assay to test the viability of Psome on LX-2 cells.

To find the therapeutic index of our MMPsome the maximum viable concentration needs to be found. The therapeutic index in defined at the window between the minimum effective dose and the maximum toxic dose. With ABA the maximum toxic concentration (MTC) can be found. A wide variety of concentrations

non-decorated Psome is used to find this dose, since it is hypothesized that the MTC of the Psome and MMPsome are close and non-decorated Psome is less expensive and labor-intensive to prepare. A range of concentrations that comprise the MTC of Psome are displayed in **Figure 9**, "Viability Psome". The lowest concentrations Psome 0.25 and 0.5 are viable with a percentage of 101 and 86% respectively. The highest concentrations Psome 2.5 and 5.0 are non-viable with a percentage of 15% and 1% respectively. Psome 1.0 has questionable viability with 63%. 63% is below the cut-off of 70%, but this concentration will be used to test if the MTC of MMPsome is as hypothesized close to the MTC of Psome and to demonstrate the dose dependent efficiency with three different concentrations.

Consequently, an ABA is performed with MMPsome in with the same concentration, to test the viability. Results of Psome and MMPsome are displayed in **Figure 9**, "Viability Psome and MMPsome. All concentrations are viable above 70%. The hypothesis that the MTC of Psome and MMPsome are close is correct, however MMPsome shows higher viability than Psome at high concentration (1.0). Since this highest concentration is also viable, this range of concentrations is used during the efficacy tests.

5.3 qPCR

5.3.1 Fibrotic markers

The choice of genes is based on the gene expression omnibus (GEO), an online database that where the expression of gene in different types of diseases is compared to the expression in healthy patients. For this project the accession GSE14323 and platform GPL 571 were used. GSE 14323 is a group of patients divided in a healthy sub-group, a cirrhotic subgroup, cirrhotic HCC sub-group and HCC subgroup. We only included the healthy and cirrhotic subgroup to find genes that can demonstrate the difference between healthy and cirrhotic/fibrotic gene expression (41). Data shown in **Figure 20**. Based on these results we decided to use coll-1, coll-3 and α-SMA as our fibrotic markers.

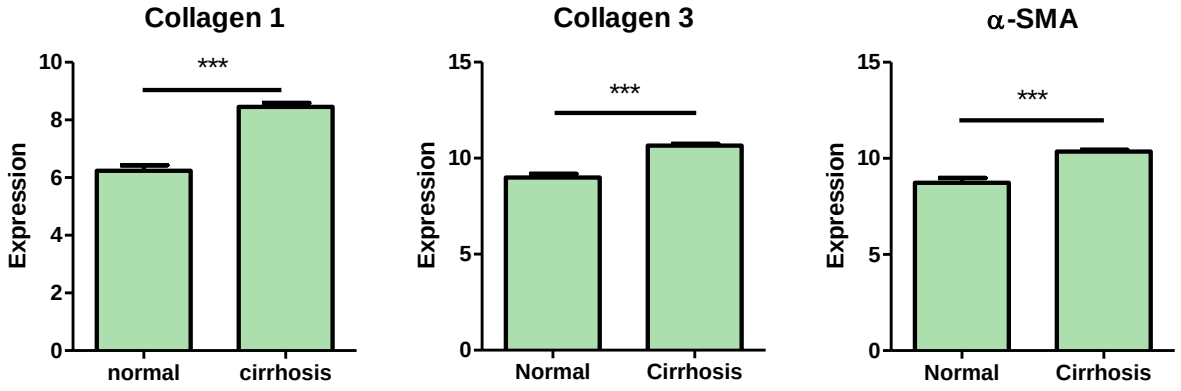

Figure 20. *Expression of three fibrotic genes based on the results collected by GEO, accession GSE 14323, platform GPL 571. Significant difference is present in all three genes calculated with an unpaired t-test, CI 95%, p<0.001.*

In **Figure 10** coll-1 showed to be a very useful marker, with significant difference between our control and TGF-β stimulated sample. Furthermore, free MMP-1 shows significant decrease in the highest two concentrations, meaning that free MMP-1 indeed attenuates fibrosis, based on these results. The Psome also shows significant difference, however there is no dose dependent response, making it more difficult to draw a conclusion on the effect of Psome on fibrosis. MMPsome only shows significant decrease in MMPsome (0.5), indicating that MMPsome can indeed help attenuate fibrosis, but there is need for more supporting data.

Coll-3 is a less widely used gene to be tested in fibrosis, but as discussed in the introduction is upregulated in fibrosis. There is no significant difference between ctrl an TGF-β visible, the outcome of ctrl normalized to TGF-β had great variety within different experiments. However, the decrease of coll-3 as a response to the therapy is remarkable. MMP-1, especially the highest concentration shows a decrease with high significance. Indicating that coll-1 and coll-3 degradation in the ECM influences the production of new collagen. The Psome also has a kind of dose dependent response on the gene expression of coll-3, even though the significance does not follow this trend. MMPsome has a great dose-dependent response that is in line with the significance, indicating that it is not just the Psome, reducing the coll-3 expression. From this gene we can conclude that MMPsome has the best dose-dependent response in decreasing the coll-3 production.

Lastly, also in α-SMA the hypothesis that the expression would be higher in the fibrotic model is not confirmed. In literature it can be found that α-SMA is an inconsistent fibrotic marker for TGF-β induced lung and kidney fibrosis (42). It is possible that besides these types of fibrosis, it is also an inconsistent marker for TGF-β induced liver fibrosis, explaining the decrease in expression in the TGF-β activated model. However, the results of the therapy treated samples are in line with the earlier discussed results, that MMPsome shows the best dose-dependent significant results. Since α-SMA is an inconsistent marker in our fibrotic model, we can not draw conclusions from this gene alone. However, it can help support the other collected data.

Taken everything into account, concluding from the three fibrotic markers used in this experiment the highest two concentrations of MMPsome (MMPsome (0.5) and (1.0)) show the most stable and fibrosis reducing results.

5.3.2 MMP1- and TIMP-1 expression

As explained earlier, fibrosis is the excessive accumulation of ECM, mainly caused by a disbalance in deposition and degradation. The degradation in fibrosis is inhibited by a decreased expression of MMP-1, and an increased expression of TIMP-1 (20). This is in line with our data, as displayed in **Figure 11**, MMP-1 expression is significantly decreased, while the TIMP-1 expression is significantly increased. The ratio of MMP-1 and TIMP-1 shows the healthy balance of MMP-1 and TIMP-1 in the healthy sample, compared to a disrupted balance in TGF-β, where the expression of MMP1 compared to TIMP-1 is significantly lower and thereby favors accumulation, fibrogenesis, over decomposition, fibrolysis.

The expression of MMP-1 shows a dose dependent increase of all treatments, which is as hypothesized in MMP-1 and MMPsome treated samples. Due to the degradation of ECM by MMP-1 the cells also start to secrete MMP-1, favoring fibrolysis. From this figure it is stated that the increase is highest in MMPsome, which is therefore, concluding from this data set the best treatment. The error bars are quite high, due to large differences in expression over different experiments. The TIMP-1 expression is also increased in most samples. This is as expected, since the TIMP-1 expression is related to the MMP-1 expression. Since both genes have an increased expression it is important that the ratio of MMP-1 and TIMP-1 is also clearly, to discover if our treatment indeed favors fibrolysis over fibrogenesis. As clearly visible in **Figure 11** MMPsome (1.0) has the highest ratio of MMP1/TIMP, even higher than the ctrl, indicating that there is indeed fibrolysis in this sample.

Based on these results and especially the restored ration of MMP-1 and TIMP-1 expression we can concluded that MMPsome (1.0) is a successful treatment, that favors fibrolysis

5.4 Western blot

Beside the gene expression, it is also important to measure the protein expression of different fibrotic markers. The chosen proteins are α-SMA and coll-1, overlapping with the genes chosen for PCR. The only significant result visible in α-SMA, shown in **Figure 12** is the significant decrease of Psome, compared to the TGF-β activated sample. There is no (significant) increase of α-SMA in TGF-β compared to the ctrl. As discussed in the previous paragraph, can it be found in literature that α-SMA is an inconsistent marker for TGF-β induced fibrosis (42). This is in line with our results, since there is no significant increase of α-SMA expression in the TGF-β activated sample. Therefore, we dismiss these results and focus on the expression of coll-1.

Coll-1, in contrast with α-SMA, shows a high significant ($P<0.001$) increase in the TGF-β activated sample, compared to the ctrl. Free MMP-1 shows a dose dependent decrease, however, without significance difference with TGF-β. The only significant difference is the increase compared to the ctrl. On the other hand, Psome and MMPsome show a dose dependent decrease with significance compared to TGF-β. Especially in the MMPsome (1.0), the expression of coll-1 is very similar to the ctrl. Meaning, that coll-1 is indeed degraded and similar to the healthy state.

Concluding from the WB, MMPsome (1.0) successfully degrades coll-1, resulting in a protein expression similar to the healthy ctrl.

5.5 Contractility assay

Under physiological circumstances, ergo the healthy control, cells do not contract, during fibrosis, ergo in the TGF-β activated samples, the cells contract. The hypothesis for MMP-1 treated cells was that with increasing concentration the contraction would lower. However, the data, shown in **Figure 13**, clearly showed a dose dependent response of circle reduction. The explanation for this phenomenon was found in the function of MMP-1. Since the function of MMP-1 is degrading collagen I, the collagen matrix was digested. Since the circle of the treated samples are smaller than the most contracted sample (TGF-β activated), the digestion is faster than potential contraction of the treated samples. Therefore, the set-up of this experiment is not suitable. However, we can conclude that the MMP-1 we use is able to digest a cell containing collagen matrix.

To overcome the problem of collagen degradation by MMP-1, an alternative set-up, explained in the methods and materials chapter was used (38).

No contraction was visible in the TGF-β stimulated samples, nor in other samples (data not shown). A possible explanation is that the removal of TGF-β stimulus inhibits the fibrosis progression and regression of fibrosis is established, thereby, decreasing the contraction to a non-visible minimum. This set-up to was insufficient to measure the contraction of non-treated and treated samples.

5.6 Wound healing assay

5.6.1 Manual WHA

A WHA was performed to quantify the level of fibrosis at a functional level, by comparing the migration, or healing, at 24 or 48 h after scratching. Again, we used a negative control (non-activated HSCs) to mimic the healthy situation and a positive control (TGF-β activated HSCs) to mimic the fibrosis situation. Furthermore, we treated the fibrosis mimic with MMP-1, Psome or MMPsome at different concentrations to evaluate the best treatment. The absolute healing is the absolute decrease of the width. The relative healing can be calculated by comparing it to the healing of the TGF-β activated healing, which will be the

highest and thereby set to 100%. These results are visualized in **Figure 15**. Here it is clearly visible that the wound healing in the TGF-β sample is higher than in the healthy control, which is in line with literature (43). After 24 h the significance is $p<0.05$ while after 48 h the significance is $p<0.001$.

For the MMP-1 treated samples, after 24 h as well as after 48 h, a dose dependent response is visible. Of which only the highest concentration has significant difference. This significance increases over time, an explanation for this could be that since all the samples start with a scratch of more or less the same width, but different wound healing rates, after a longer period the difference in width of scratch is higher.

As visible in the figure, there is no error bar at the highest concentration of Psome. Due to apoptosis of some cells, it was not possible to mark the point of migration of the living cells. Therefore, the WHA of Psome (1.0) was not performed in triplicate and therefore has no error bar. There is no dose dependent response of Psome visible in this experiment, which is in line with the hypothesis that the Psome itself does not attenuates fibrosis. However, we can see that the middle concentration has significantly lower wound healing.

There is a clear dose dependent response visible in the MMPsome treated samples after 24h and 48h. Also, the significance increases in time and concentration. At 24h we can also see a significant decrease between the control and the highest sample of MMP and MMPsome. This is not favorable, since it might be harmful if the liver is not able to heal injuries due to therapy. Wound healing to some point is necessary for healthy liver regeneration after injury. At 48 h the MMPsome is not significant with the control, while there is a significant difference between the TGF-β activated sample. This is a favorable response of therapy.

Since the width of a WHA is measured by the researcher himself or herself, it is not completely objectively measured. The exact line where the scratch begins is difficult to draw and the width can therefore differ per measurer. Also, when the same picture is measured by the same measurer repeatably, outcomes can differ. Taken this together, a WHA done in this way is subjective.

5.6.2 WHA performed using CytoSMART™ Omni

We had the opportunity to use the CytoSMART™ Omni. This live-cell imager is equipped with software that can identify a scratch and can accurately measure the surface of the scratch. Besides, it can make pictures every hour, inside the incubator, making it unnecessary to remove the optimal conditions by making pictures outside the incubator every 24 h. Since the software can identify the scratch surface accurately, it can also measure the decrease of this surface over time, more accurately and less subjective.

Results of this experiments are displayed in **Figure 16** en **Figure 17**. Since the area is measured by a computer instead of manually, it is done more objectively. Also, the cells remain in the incubator during the whole experiment, instead of being moved, shaken and handled outside during the manual picturing. Therefore, this automatic picturing ensures optimal conditions. The data shown in **Figure 17** does not show any significance. Significance is not calculated since only one replicate is made, because the CytoSMART™ Omni was used as a pilot test. More measurements should be performed for higher reliability. However, this data together with the manually retrieved data suggest that MMPsome is the best treatment, which is in line with previous findings.

5.7 In and ex vivo mouse model study

5.7.1 Liver-to-body weight

CCl_4 induced fibrotic mouse models are associated with increased liver-to-body weight (44). Also, in our study we found a significant increase of liver-to-body weight, demonstrated in **Figure 18**. MMP-1 did not decrease the liver-to-body weight as expected. It was hypothesized that free MMP-1 would be degraded, before accessing the liver, this is in line with the results in **Figure 18**. MMPsomes on the other hand show a decrease in liver-to-body weight compared to the CCl_4 group. There is no significant difference between MMPsome and healthy, nor between MMPsome and CCl_4. There is regression of fibrosis visible, based on these results, however no resolution.

5.7.2 Ex vivo staining

All samples show living cell without a lot of apoptosis or necrosis, visualized in **Figure 19**. In the MMP-1 as well as the MMPsome treated samples, show more gaps in the ECM, compared to the serum treated sample and Psome treated. It is possible these gaps are formed by digested coll-1, meaning that this enzyme is able to digest liver tissue ECM. Free MMP-1 seems more effective in the *ex vivo* study. Since free MMP-1 is smaller in size than decorated MMP-1, it can more easily translocate into the core of the *ex vivo* liver and thereby faster digest the coll-1 everywhere throughout the sample. From the first visual analysis we can state that the data show promising results, however the quantification yet has to be done.

5.8 Impact of this study

Decoration enables non-triggered drug availability, while guaranteeing protection. In our research, a state-of-the-art decoration of a therapeutic agent, MMP-1, on the outer surface of a DDS, Psome is proven possible. Besides, we ascertained that the MMP is protected from activity loss and degradation, even though the enzyme is on the outer surface of the Psome. Reasons to choose Psomes as DDS are their wide tunability and easy preparations properties (24). However, drug release is always an issue you encounter when choosing a DDS. An advantage of pH-responsive Psomes is their pH-triggered releasing potential. When taken-up by cells, or inside a tumor environment, the pH is decreased and release of encapsulated small molecules is triggered. However, when a trigger does not present itself, for example in extracellular targeting, release remains difficult (45). With our MMPsome the difficulty of release is evaded. The therapeutic compound is directly available on the outer side of the DDS.

We restored the MMP-TIMP balance without viral vector gene delivery. Imuro et al. and Du et al. also showed fibrosis resolution by restoring the MMP-TIMP balance, however used, possible immunogenic and toxic viral vectors (14,17). Besides, due to chronic MMP-1 overexpression by gene delivery, over degradation is possible (10,23). Since our study does not use viral vectors, we will not encounter problems based on these immunogenic viral vectors. Moreover, we can influence the amount of MMP expression by increasing or decreasing the dose, preventing chronic overexpression.

Chapter 6 Conclusion and future perspectives

This chapter will summarize and conclude all findings of the research and explain future perspectives

6.1 conclusions

Before we discuss the concluding remarks, we need to go back to our aim. The first aim of our research was to develop a Psome with MMP-1 decorated on the outer surface, the MMPsome. A state-of-the-art protocol for easy manufacturing of the MMPsome is established in Dresden at IPF. The size, PDI and ζ-potential are used to prove decoration. Increase of size and PDI and decrease of ζ-potential have indeed proven successful decoration of MMP-1 on the outer surface of the Psome. Furthermore, decoration efficiency is measured by comparing the intensity of RhB labelled MMP-1 before and after purification by dialysis. Due to the drainage of free MMP-1 during dialysis, the decoration efficiency could be calculated and is established to be 30%. Besides it is shown that the Psome is able to protect the MMP-1 from activity loss. Free MMP-1 loses activity when not stored under optimal conditions, at -20°C. However, decorated enzyme can be stored at room temperature for 1 week without too much loss of activity. Altogether, we established an easy protocol for development of a robust MMPsome with enzyme activity protection.

This robust MMPsome was developed as treatment of liver fibrosis. To establish if the MMPsome is indeed suitable as therapeutic, *in vitro* experiments have to be performed. First of all, it is important to find the therapeutic index of a therapeutic compound. Using a viability assay, ABA, we found the maximum toxic concentration of the MMPsome. This and lower concentrations were used to test fibrolytic effect. First of all, the gene and protein expression of fibrotic marker significantly decreased in MMPsome treated samples, compared to non-treated, free MMP-1 treated and Psome treated samples. The coll-1 expression reduced to physiological amounts. Furthermore, the ratio of MMP-1 and TIMP-1 was increased to higher than physiological, indicating successful decomposition of ECM, ergo fibrolysis. Besides, we have proven that the MMP-1 used in this study is able to degrade a 3D cell-containing collagen matrix, during our contractility assay. Lastly, a functionality assay, a wound healing assay was performed. Again, here we found that the MMPsome was the most successful therapeutic, by decreasing the fibrotic wound healing. So, all our *in vitro* experiments pointed out that our MMPsome was the most successful therapeutic for regression of fibrosis.

Beside the *in vitro* experiments, *in* and *ex vivo* studies were performed to demonstrate the therapeutic effect of the MMPsome. A CCl_4 acute fibrosis induced mouse model was used to test the therapeutic effect compared to wild-type mice and MMP-1 treated mice. The reduction is liver-to-body weight and visual analysis of the staining are promising results, but further analysis has to be performed.

To conclude, after successful fabrication of MMPsomes, the MMPsome showed to be a promising therapeutic strategy for the treatment of liver fibrosis.

6.2 Future perspectives

Besides being a promising therapy in liver fibrosis, an MMPsome could be used for other purposes. MMP-1 is gaining popularity as an anti-cancer therapy. For example, pancreatic ductal adenocarcinoma (PDAC) is a very aggressive cancer type with a five-year survival rate below 8%. No therapy has been found successful, as no therapy is able to penetrate through the close collagen-rich stroma. Zinger et al. have focused on dual therapy, where first the patient is treated with liposomes containing MMP-1 to reduce the tumor stroma, after which the patient is treated with chemotherapy to reduce the tumor itself (46). MMPsomes could be used to improve this concept. A small size therapeutic compound could be

encapsulated in the Psome, which will be decorated with MMP-1 thereafter. Due to enhanced permeability and retention effect (EPR) in a tumor environment, the MMPsome can accumulate in the tumor environment via passive targeting (47). There, the decorated MMP-1 on the outer surface of the Psome will degrade the collagen-rich stroma. Due to digestion of the stroma, the MMPsome can enter the tumor tissue, which has a lower pH (48). Due to this pH drop, the Psome will swell and the small anti-cancer drug can reduce the tumor. The idea is visualized in **Figure 21**.

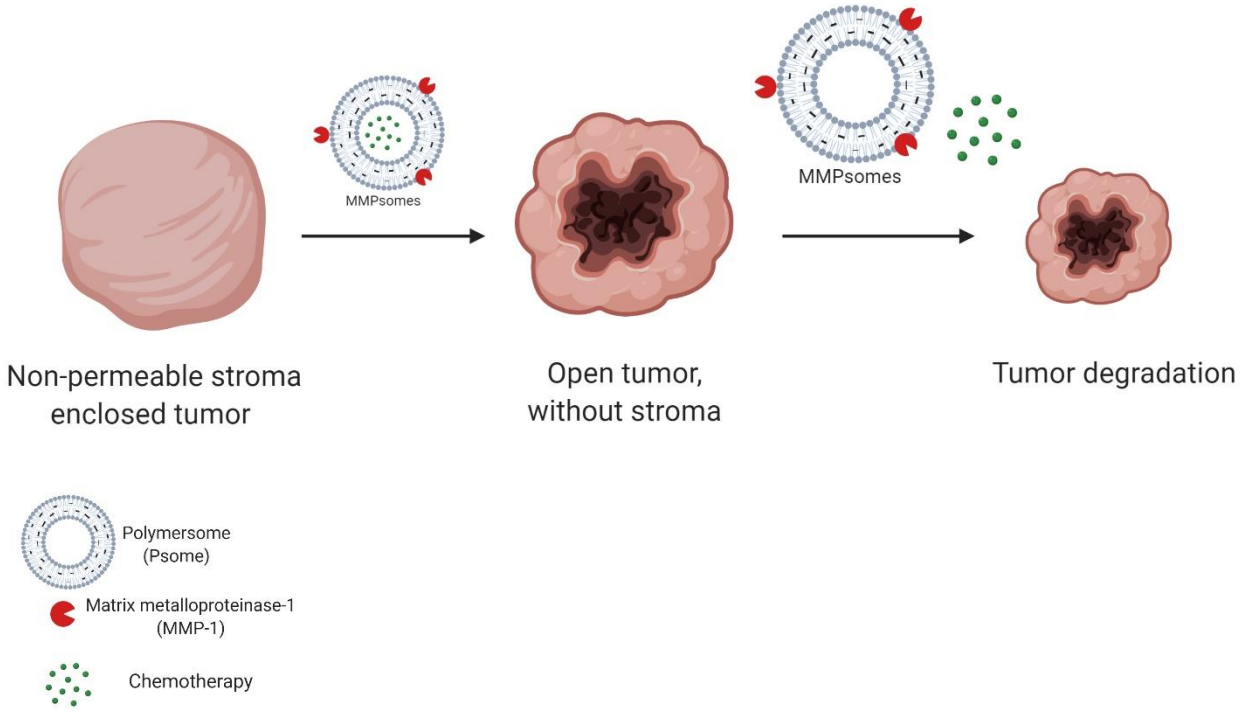

***Figure 21**. MMPsome encapsulating chemotherapy accumulates around the tumor due to EPR. Here, the MMP-1 can degrade the collagen-rich stroma and the MMPsome enters the tumor. Here the MMPsome swell due to pH drop and release the chemotherapy, which degrades the tumor.*

Not only for PDAC this could be a promising therapy also in other encapsulated tumors MMPsome could increase the therapeutic effect by targeted delivery of the anti-cancer drug.

Chapter 7 Future Recommendation

First of all, I recommend to use the data obtained from the CCl_4 acute fibrotic mouse model and analyze this data. Furthermore, repeating the experiments performed using the CytoSmart^{tm} Omni, for higher reliability. Besides, I recommend to perform new *in vivo* experiments on different mouse models. To test if the MMPsome is also functional in ALD, NAFLD and hepatitis induced fibrosis. In these studies I also advise to use multiple treatment injections, since these studies represent chronic fibrosis, in contrast with our acute fibrosis model. These are recommendations based on MMPsomes as therapeutic strategy in liver fibrosis.

Beyond this scope, I think our MMPsomes have brother therapeutic perspectives, especially in cancer therapy described in future perspectives. Besides PDAC (46), also hepatocellular carcinoma (HCC) (49) and mamma carcinoma (50) can be encapsulated by collagen rich stroma, inhibiting the drug efficacy. Therefore, I recommend tumor-on-a-chip drug testing. Tumor-on-a-chip gains popularity by minimizing animal drug testing and higher tunability of the specific tumor features. The important features as stroma encapsulation can be incorporated in a tumor on a chip, making drug testing more efficient (51,52). I recommend collaboration with tumor-on-a-chip researchers who can design one or multiple specific stroma encapsulating tumors, for drug testing of our MMPsome, encapsulating chemotherapeutic drugs.

References

1. Schuppan D, Afdhal NH. Liver cirrhosis. Lancet [Internet]. 2008 Mar 8 [cited 2019 Feb 27];371(9615):838–51. Available from: https://www.sciencedirect.com/science/article/pii/S0140673608603839

2. Pimpin L, Cortez-Pinto H, Negro F, Corbould E, Lazarus J V., Webber L, et al. Burden of liver disease in Europe: Epidemiology and analysis of risk factors to identify prevention policies. J Hepatol [Internet]. 2018 Sep 1 [cited 2019 Feb 27];69(3):718–35. Available from: https://www.sciencedirect.com/science/article/pii/S0168827818320579

3. Pimpin L, Webber L, Sacton J, Corbould E, Flood J. Project Report Risk Factors and the Burden of Liver Disease in Europe and Selected Central Asian Countries [Internet]. 2018 [cited 2019 Feb 27]. Available from: http://www.easl.eu

4. Blachier M, Leleu H, Peck-Radosavljevic M, Valla D-C, Roudot-Thoraval F. The burden of liver disease in Europe: A review of available epidemiological data. J Hepatol [Internet]. 2013 Mar 1 [cited 2019 Feb 27];58(3):593–608. Available from: https://www.sciencedirect.com/science/article/pii/S0168827812009245

5. Omar R, Yang J, Liu H, Davies NM, Gong Y. Hepatic Stellate Cells in Liver Fibrosis and siRNA-Based Therapy. In Springer, Cham; 2016 [cited 2019 Feb 27]. p. 1–37. Available from: http://link.springer.com/10.1007/112_2016_6

6. Puche JE, Saiman Y, Friedman SL. Hepatic Stellate Cells and Liver Fibrosis. In: Comprehensive Physiology [Internet]. Hoboken, NJ, USA: John Wiley & Sons, Inc.; 2013 [cited 2019 Feb 27]. p. 1473–92. Available from: http://doi.wiley.com/10.1002/cphy.c120035

7. Xu F, Liu C, Zhou D, Zhang L. TGF-β/SMAD Pathway and Its Regulation in Hepatic Fibrosis. J Histochem Cytochem [Internet]. 2016 Mar 8 [cited 2019 Mar 1];64(3):157–67. Available from: http://journals.sagepub.com/doi/10.1369/0022155415627681

8. Bansal R, Nagórniewicz B, Prakash J. Clinical Advancements in the Targeted Therapies against Liver Fibrosis. Mediators Inflamm [Internet]. 2016 Nov 24 [cited 2019 Mar 11];2016:1–16. Available from: https://www.hindawi.com/journals/mi/2016/7629724/

9. Naim A, Pan Q, Baig MS. Matrix Metalloproteinases (MMPs) in Liver Diseases. J Clin Exp Hepatol [Internet]. 2017 Dec 1 [cited 2019 Feb 27];7(4):367–72. Available from: https://www.sciencedirect.com/science/article/pii/S0973688317304619

10. Iimuro Y, Brenner DA. Matrix metalloproteinase gene delivery for liver fibrosis. Pharm Res [Internet]. 2008 Feb [cited 2019 Feb 20];25(2):249–58. Available from: http://www.ncbi.nlm.nih.gov/pubmed/17577645

11. Liu T, Wang P, Cong M, Zhang D, Liu L, Li H, et al. Matrix metalloproteinase-1 induction by diethyldithiocarbamate is regulated via Akt and ERK/miR222/ETS-1 pathways in hepatic stellate cells. Biosci Rep [Internet]. 2016 Aug 1 [cited 2019 Feb 27];36(4):e00371. Available from: http://www.ncbi.nlm.nih.gov/pubmed/27412967

12. Cheng Q, Li C, Yang C, Zhong Y, Wu D, Shi L, et al. Methyl ferulic acid attenuates liver fibrosis and hepatic stellate cell activation through the TGF-β1/Smad and NOX4/ROS pathways. Chem Biol Interact [Internet]. 2019 Feb [cited 2019 Mar 1];299:131–9. Available from: https://linkinghub.elsevier.com/retrieve/pii/S0009279718310706

13. Okazaki I, Watanabe T, Hozawa S, Niioka M, Arai M, Maruyama K. Reversibility of hepatic fibrosis: From the first report of collagenase in the liver to the possibility of gene therapy for recovery. Keio J Med [Internet]. 2001 [cited 2019 Feb 27];50(2):58–65. Available from: http://joi.jlc.jst.go.jp/JST.Journalarchive/kjm1952/50.58?from=CrossRef

14. Du C, Jiang M, Wei X, Qin J, Xu H, Wang Y, et al. Transplantation of human matrix metalloproteinase-1 gene-modified bone marrow-derived mesenchymal stem cell attenuates CCL4-induced liver fibrosis in rats. Int J Mol Med [Internet]. 2018 Feb 27 [cited 2019 Feb 27];41(6):3175–84. Available from: http://www.spandidos-publications.com/10.3892/ijmm.2018.3516

15. Wiegand J, Berg T. The etiology, diagnosis and prevention of liver cirrhosis: part 1 of a series on liver cirrhosis. Dtsch Arztebl Int [Internet]. 2013 Feb [cited 2019 Feb 27];110(6):85–91. Available from: http://www.ncbi.nlm.nih.gov/pubmed/23451000

16. Goldberg D, Ditah IC, Saeian K, Lalehzari M, Aronsohn A, Gorospe EC, et al. Changes in the Prevalence of Hepatitis C Virus Infection, Nonalcoholic Steatohepatitis, and Alcoholic Liver Disease Among Patients With Cirrhosis or Liver Failure on the Waitlist for Liver Transplantation. Gastroenterology [Internet]. 2017 Apr 1 [cited 2019 Feb 28];152(5):1090-1099.e1. Available from: https://www.sciencedirect.com/science/article/pii/S0016508517300148

17. Iimuro Y, Nishio T, Morimoto T, Nitta T, Stefanovic B, Choi SK, et al. Delivery of matrix metalloproteinase-1 attenuates established liver fibrosis in the rat. Gastroenterology [Internet]. 2003 Feb 1 [cited 2019 Feb 25];124(2):445–58. Available from: https://www.sciencedirect.com/science/article/pii/S0016508502159142

18. GROSS J, LAPIERE CM. Collagenolytic activity in amphibian tissues: a tissue culture assay. Proc Natl Acad Sci U S A [Internet]. 1962 Jun 15 [cited 2019 Aug 15];48(6):1014–22. Available from: http://www.ncbi.nlm.nih.gov/pubmed/13902219

19. Duarte S, Baber J, Fujii T, Coito AJ. Matrix metalloproteinases in liver injury, repair and fibrosis. Matrix Biol [Internet]. 2015 May 1 [cited 2019 Aug 15];44–46:147–56. Available from: https://www.sciencedirect.com/science/article/pii/S0945053X15000050

20. Roeb E. Matrix metalloproteinases and liver fibrosis (translational aspects). Matrix Biol [Internet]. 2018 Aug 1 [cited 2019 Oct 7];68–69:463–73. Available from: https://www.sciencedirect.com/science/article/pii/S0945053X17303530

21. Roderfeld M. Matrix metalloproteinase functions in hepatic injury and fibrosis. Matrix Biol [Internet]. 2018 Aug 1 [cited 2019 Sep 3];68–69:452–62. Available from: https://www.sciencedirect.com/science/article/pii/S0945053X17303505?via%3Dihub

22. Fellows CR, Matta C, Zakany R, Khan IM, Mobasheri A. Adipose, Bone Marrow and Synovial Joint-Derived Mesenchymal Stem Cells for Cartilage Repair. Front Genet [Internet]. 2016 Dec 20 [cited 2019 Aug 28];7:213. Available from: http://journal.frontiersin.org/article/10.3389/fgene.2016.00213/full

23. Eom YW, Shim KY, Baik SK. Mesenchymal stem cell therapy for liver fibrosis. Korean J Intern Med [Internet]. 2015 Sep [cited 2019 Aug 28];30(5):580–9. Available from: http://www.ncbi.nlm.nih.gov/pubmed/26354051

24. Onaca O, Enea R, Hughes DW, Meier W. Stimuli-Responsive Polymersomes as Nanocarriers for Drug and Gene Delivery. Macromol Biosci [Internet]. 2009 Feb 11 [cited 2019 Feb 27];9(2):129–39. Available from: http://doi.wiley.com/10.1002/mabi.200800248

25. Balasubramanian V, Herranz-Blanco B, Almeida P V., Hirvonen J, Santos HA. Multifaceted polymersome platforms: Spanning from self-assembly to drug delivery and protocells. Prog Polym Sci [Internet]. 2016 Sep 1 [cited 2019 Feb 27];60:51–85. Available from: https://www.sciencedirect.com/science/article/pii/S0079670016300132

26. Liao J, Wang C, Wang Y, Luo F, Qian Z. Recent Advances in Formation, Properties, and Applications of Polymersomes. Curr Pharm Des [Internet]. 2012 Aug 1 [cited 2019 Feb 27];18(23):3432–41. Available from: http://openurl.ingenta.com/content/xref?genre=article&issn=1381-6128&volume=18&issue=23&spage=3432

27. Anajafi T, Mallik S. Polymersome-based drug-delivery strategies for cancer therapeutics. Ther Deliv [Internet]. 2015 Apr 21 [cited 2019 Feb 27];6(4):521–34. Available from: http://www.future-science.com/doi/10.4155/tde.14.125

28. Gaitzsch J, Appelhans D, Wang L, Battaglia G, Voit B. Synthetic Bio-nanoreactor: Mechanical and Chemical Control of Polymersome Membrane Permeability. Angew Chemie Int Ed [Internet]. 2012 Apr 27 [cited 2019 Feb 27];51(18):4448–51. Available from: http://doi.wiley.com/10.1002/anie.201108814

29. Liu X, Formanek P, Voit B, Appelhans D. Functional Cellular Mimics for the Spatiotemporal Control of Multiple Enzymatic Cascade Reactions. Angew Chemie Int Ed [Internet]. 2017 Dec 18 [cited 2019 Feb 27];56(51):16233–8. Available from: http://doi.wiley.com/10.1002/anie.201708826

30. Gräfe D, Gaitzsch J, Appelhans D, Voit B. Cross-linked polymersomes as nanoreactors for controlled and stabilized single and cascade enzymatic reactions. Nanoscale [Internet]. 2014 Aug 21 [cited 2019 Feb 27];6(18):10752–61. Available from: http://xlink.rsc.org/?DOI=C4NR02155J

31. Gumz H, Lai TH, Voit B, Appelhans D. Fine-tuning the pH response of polymersomes for mimicking and controlling the cell membrane functionality. Polym Chem [Internet]. 2017 May 16 [cited 2019 Feb 27];8(19):2904–8. Available from: http://xlink.rsc.org/?DOI=C7PY00089H

32. Iyisan B, Kluge J, Formanek P, Voit B, Appelhans D. Multifunctional and Dual-Responsive Polymersomes as Robust Nanocontainers: Design, Formation by Sequential Post-Conjugations, and pH-Controlled Drug Release. Chem Mater [Internet]. 2016 Mar 8 [cited 2019 Feb 27];28(5):1513–25. Available from: http://pubs.acs.org/doi/10.1021/acs.chemmater.5b05016

33. Iyisan B, Siedel AC, Gumz H, Yassin M, Kluge J, Gaitzsch J, et al. Dynamic Docking and Undocking Processes Addressing

Selectively the Outside and Inside of Polymersomes. Macromol Rapid Commun [Internet]. 2017 Nov 1 [cited 2019 Feb 27];38(21):1700486. Available from: http://doi.wiley.com/10.1002/marc.201700486

34. Gumz H, Boye S, Iyisan B, Krönert V, Formanek P, Voit B, et al. Toward Functional Synthetic Cells: In-Depth Study of Nanoparticle and Enzyme Diffusion through a Cross-Linked Polymersome Membrane. 2019 [cited 2019 Feb 27]; Available from: www.advancedscience.com

35. Sigma-Aldrich. Collagenase from Clostidium histolyticum [Internet]. 2019 [cited 2019 Apr 15]. Available from: https://www.sigmaaldrich.com/catalog/product/sigma/c0130?lang=en&region=NL

36. Xu L, Hui AY, Albanis E, Arthur MJ, O'Byrne SM, Blaner WS, et al. Human hepatic stellate cell lines, LX-1 and LX-2: new tools for analysis of hepatic fibrosis. Gut [Internet]. 2005 Jan 1 [cited 2019 Feb 28];54(1):142–51. Available from: http://www.ncbi.nlm.nih.gov/pubmed/15591520

37. Scholten D, Trebicka J, Liedtke C, Weiskirchen R. The carbon tetrachloride model in mice. Lab Anim. 2015;49:4–11.

38. Kobayashi T, Kim HJ, Liu X, Sugiura H, Kohyama T, Fang Q, et al. Matrix metalloproteinase-9 activates TGF-β and stimulates fibroblast contraction of collagen gels. Am J Physiol - Lung Cell Mol Physiol. 2014 Jun 1;306(11).

39. 000664 - C57BL/6J [Internet]. [cited 2019 Nov 26]. Available from: https://www.jax.org/strain/000664

40. Rampersad SN. Multiple applications of alamar blue as an indicator of metabolic function and cellular health in cell viability bioassays. Sensors (Switzerland). 2012 Sep;12(9):12347–60.

41. GEO2R - GEO - NCBI [Internet]. [cited 2019 Nov 29]. Available from: https://www.ncbi.nlm.nih.gov/geo/geo2r/?acc=GSE14323&platform=GPL571

42. Sun KH, Chang Y, Reed NI, Sheppard D. α-smooth muscle actin is an inconsistent marker of fibroblasts responsible for force-dependent TGFβ activation or collagen production across multiple models of organ fibrosis. Am J Physiol - Lung Cell Mol Physiol. 2016 Mar 1;310(9):L824–36.

43. Lichtman MK, Otero-Vinas M, Falanga V. Transforming growth factor beta (TGF-β) isoforms in wound healing and fibrosis. Wound Repair Regen [Internet]. 2016 Mar [cited 2019 Nov 11];24(2):215–22. Available from: http://doi.wiley.com/10.1111/wrr.12398

44. Brol MJ, Rösch F, Schierwagen R, Magdaleno F, Uschner FE, Manekeller S, et al. Combination of CCL4 with alcoholic and metabolic injuries mimics human liver fibrosis. Am J Physiol - Gastrointest Liver Physiol. 2019 Aug 1;317(2):G182–94.

45. Singh R, Lillard JW. Nanoparticle-based targeted drug delivery. Vol. 86, Experimental and Molecular Pathology. 2009. p. 215–23.

46. Zinger A, Koren L, Adir O, Poley M, Alyan M, Yaari Z, et al. Collagenase Nanoparticles Enhance the Penetration of Drugs into Pancreatic Tumors. ACS Nano [Internet]. 2019 Sep 20 [cited 2019 Oct 1];acsnano.9b02395. Available from: http://www.ncbi.nlm.nih.gov/pubmed/31503443

47. Iyer AK, Khaled G, Fang J, Maeda H. Exploiting the enhanced permeability and retention effect for tumor targeting. Vol. 11, Drug Discovery Today. 2006. p. 812–8.

48. Zhang X, Lin Y, Gillies RJ. Tumor pH and its measurement. Vol. 51, Journal of Nuclear Medicine. 2010. p. 1167–70.

49. Ng IOL, Lai ECS, Fan ST, Ng MMT. Tumor encapsulation in hepatocellular carcinoma. A pathologic study of 189 cases. Cancer. 1992;70(1):45–9.

50. Raviraj V, Zhang H, Chien HY, Cole L, Thompson EW, Soon L. Dormant but migratory tumour cells in desmoplastic stroma of invasive ductal carcinomas. Clin Exp Metastasis. 2012 Mar;29(3):273–92.

51. Tsai HF, Trubelja A, Shen AQ, Bao G. Tumour-on-a-chip: Microfluidic models of tumour morphology, growth and microenvironment. Vol. 14, Journal of the Royal Society Interface. Royal Society Publishing; 2017.

52. Wang Y, Cuzzucoli F, Escobar A, Lu S, Liang L, Wang S. Tumor-on-a-chip platforms for assessing nanoparticle-based cancer therapy. Vol. 29, Nanotechnology. Institute of Physics Publishing; 2018.

53. Murawaki Y, Ikuta Y, Idobe Y, Kawasaki H. Serum matrix metalloproteinase-1 in patients with chronic viral hepatitis. J Gastroenterol Hepatol [Internet]. 2002 Feb 28 [cited 2019 Oct 8];14(2):138–45. Available from:

http://doi.wiley.com/10.1046/j.1440-1746.1999.01821.x

54. Lichtinghagen R, Bahr MJ, Wehmeier M, Michels D, Haberkorn CI, Arndt B, et al. Expression and coordinated regulation of matrix metalloproteinases in chronic hepatitis C and hepatitis C virus-induced liver cirrhosis. Clin Sci (Lond) [Internet]. 2003 Sep 1 [cited 2019 Sep 10];105(3):373–82. Available from: http://www.ncbi.nlm.nih.gov/pubmed/12760742

55. Takahara T, Furui K, Yata Y, Jin B, Zhang L, Nambu S, et al. Dual expression of matrix metalloproteinase-2 and membrane-type 1-matrix metalloproteinase in fibrotic human livers. Hepatology [Internet]. 1997 Dec 1 [cited 2019 Sep 10];26(6):1521–9. Available from: https://www.sciencedirect.com/science/article/pii/S0270913997005387

56. Radbill BD, Gupta R, Ramirez MCM, DiFeo A, Martignetti JA, Alvarez CE, et al. Loss of Matrix Metalloproteinase-2 Amplifies Murine Toxin-Induced Liver Fibrosis by Upregulating Collagen I Expression. Dig Dis Sci [Internet]. 2011 Feb 19 [cited 2019 Sep 10];56(2):406–16. Available from: http://link.springer.com/10.1007/s10620-010-1296-0

57. Onozuka I, Kakinuma S, Kamiya A, Miyoshi M, Sakamoto N, Kiyohashi K, et al. Cholestatic liver fibrosis and toxin-induced fibrosis are exacerbated in matrix metalloproteinase-2 deficient mice. Biochem Biophys Res Commun [Internet]. 2011 Mar 4 [cited 2019 Sep 10];406(1):134–40. Available from: https://www.sciencedirect.com/science/article/pii/S0006291X11001951

58. Prystupa A, Boguszewska-Czubara A, Bojarska-Junak A, Toruń-Jurkowska A, Roliński J, Załuska W. Activity of MMP-2, MMP-8 and MMP-9 in serum as a marker of progression of alcoholic liver disease in people from Lublin Region, eastern Poland. Ann Agric Environ Med [Internet]. 2015 May 11 [cited 2019 Sep 10];22(2):325–8. Available from: http://www.journalssystem.com/aaem/Activity-of-MMP-2-MMP-8-and-MMP-9-in-serum-nas-a-marker-of-progression-of-alcoholic-liver-disease-in-people-from-Lublin-Region-eastern-Poland,72283,0,2.html

59. CURSIO R, MARI B, LOUIS K, ROSTAGNO P, SAINT-PAUL M-C, GIUDICELLI J, et al. Rat liver injury after normothermic ischemia is prevented by a phosphinic matrix metalloproteinase inhibitor. FASEB J [Internet]. 2002 Jan 14 [cited 2019 Sep 11];16(1):93–5. Available from: http://www.fasebj.org/doi/10.1096/fj.01-0279fje

60. Huang C-C, Chuang J-H, Chou M-H, Wu C-L, Chen C-M, Wang C-C, et al. Matrilysin (MMP-7) is a major matrix metalloproteinase upregulated in biliary atresia-associated liver fibrosis. Mod Pathol [Internet]. 2005 Jul 28 [cited 2019 Sep 11];18(7):941–50. Available from: http://www.nature.com/articles/3800374

61. Bodey B, Bodey B, Siegel SE, Kaiser HE. Immunocytochemical detection of MMP-3 and -10 expression in hepatocellular carcinomas. Anticancer Res [Internet]. 2000 [cited 2019 Sep 11];20(6B):4585–90. Available from: http://www.ncbi.nlm.nih.gov/pubmed/11210857

62. Zhang M, Dai C, Zhu H, Chen S, Wu Y, Li Q, et al. Cyclophilin A promotes human hepatocellular carcinoma cell metastasis via regulation of MMP3 and MMP9. Mol Cell Biochem [Internet]. 2011 Nov 11 [cited 2019 Sep 11];357(1–2):387–95. Available from: http://link.springer.com/10.1007/s11010-011-0909-z

63. Zeng Z-S, Shu W-P, Cohen AM, Guillem JG. Matrix metalloproteinase-7 expression in colorectal cancer liver metastases: evidence for involvement of MMP-7 activation in human cancer metastases. Clin Cancer Res [Internet]. 2002 Jan 1 [cited 2019 Sep 11];8(1):144–8. Available from: http://www.ncbi.nlm.nih.gov/pubmed/11801551

64. Irvine KM, Wockner LF, Hoffmann I, Horsfall LU, Fagan KJ, Bijin V, et al. Multiplex Serum Protein Analysis Identifies Novel Biomarkers of Advanced Fibrosis in Patients with Chronic Liver Disease with the Potential to Improve Diagnostic Accuracy of Established Biomarkers. Lin H-C, editor. PLoS One [Internet]. 2016 Nov 18 [cited 2019 Sep 11];11(11):e0167001. Available from: http://dx.plos.org/10.1371/journal.pone.0167001

65. Chiu C-C, Sheu J-C, Chen C-H, Lee C-Z, Chiou L-L, Chou S-H, et al. Global gene expression profiling reveals a key role of CD44 in hepatic oval-cell reaction after 2-AAF/CCl4 injury in rodents. Histochem Cell Biol [Internet]. 2009 Nov 16 [cited 2019 Sep 11];132(5):479–89. Available from: http://link.springer.com/10.1007/s00418-009-0634-9

66. Siller-López F, Sandoval A, Salgado S, Salazar A, Bueno M, Garcia J, et al. Treatment with human metalloproteinase-8 gene delivery ameliorates experimental rat liver cirrhosis. Gastroenterology [Internet]. 2004 Apr 1 [cited 2019 Sep 11];126(4):1122–33. Available from: https://www.sciencedirect.com/science/article/pii/S0016508503021450

67. Harty MW, Huddleston HM, Papa EF, Puthawala T, Tracy AP, Ramm GA, et al. Repair after cholestatic liver injury correlates with neutrophil infiltration and matrix metalloproteinase 8 activity. Surgery [Internet]. 2005 Aug 1 [cited 2019 Sep 11];138(2):313–20. Available from: https://www.sciencedirect.com/science/article/pii/S0039606005001741

68. Van Lint P, Wielockx B, Puimège L, Noël A, López-Otin C, Libert C. Resistance of collagenase-2 (matrix metalloproteinase-8)-deficient mice to TNF-induced lethal hepatitis. J Immunol [Internet]. 2005 Dec 1 [cited 2019 Sep 11];175(11):7642–9. Available from: http://www.ncbi.nlm.nih.gov/pubmed/16301674

69. Olle EW, Ren X, McClintock SD, Warner RL, Deogracias MP, Johnson KJ, et al. Matrix metalloproteinase-9 is an important factor in hepatic regeneration after partial hepatectomy in mice. Hepatology [Internet]. 2006 Sep 1 [cited 2019 Sep 11];44(3):540–9. Available from: http://doi.wiley.com/10.1002/hep.21314

70. Zhou X, Murphy FR, Gehdu N, Zhang J, Iredale JP, Benyon RC. Engagement of alphavbeta3 integrin regulates proliferation and apoptosis of hepatic stellate cells. J Biol Chem [Internet]. 2004 Jun 4 [cited 2019 Sep 11];279(23):23996–4006. Available from: http://www.ncbi.nlm.nih.gov/pubmed/15044441

71. Moore C, Shen X-D, Gao F, Busuttil RW, Coito AJ. Fibronectin-α4β1 Integrin Interactions Regulate Metalloproteinase-9 Expression in Steatotic Liver Ischemia and Reperfusion Injury. Am J Pathol [Internet]. 2007 Feb 1 [cited 2019 Sep 12];170(2):567–77. Available from: https://www.sciencedirect.com/science/article/pii/S0002944010608802

72. Hamada T, Fondevila C, Busuttil RW, Coito AJ. Metalloproteinase-9 deficiency protects against hepatic ischemia/reperfusion injury. Hepatology [Internet]. 2007 Sep 19 [cited 2019 Sep 18];47(1):186–98. Available from: http://doi.wiley.com/10.1002/hep.21922

73. Hamada T, Duarte S, Tsuchihashi S, Busuttil RW, Coito AJ. Inducible Nitric Oxide Synthase Deficiency Impairs Matrix Metalloproteinase-9 Activity and Disrupts Leukocyte Migration in Hepatic Ischemia/Reperfusion Injury. Am J Pathol [Internet]. 2009 Jun 1 [cited 2019 Oct 1];174(6):2265–77. Available from: https://www.sciencedirect.com/science/article/pii/S0002944010610851

74. Kato H, Kuriyama N, Duarte S, Clavien P-A, Busuttil RW, Coito AJ. MMP-9 deficiency shelters endothelial PECAM-1 expression and enhances regeneration of steatotic livers after ischemia and reperfusion injury. J Hepatol [Internet]. 2014 May 1 [cited 2019 Oct 1];60(5):1032–9. Available from: https://www.sciencedirect.com/science/article/pii/S0168827814000026

75. Hori T, Uemoto S, Walden LB, Chen F, Baine A-MT, Hata T, et al. Matrix metalloproteinase-9 as a therapeutic target for the progression of fulminant liver failure with hepatic encephalopathy: A pilot study in mice. Hepatol Res [Internet]. 2014 Jun 1 [cited 2019 Oct 1];44(6):651–62. Available from: http://doi.wiley.com/10.1111/hepr.12161

76. Nguyen JH, Yamamoto S, Steers J, Sevlever D, Lin W, Shimojima N, et al. Matrix metalloproteinase-9 contributes to brain extravasation and edema in fulminant hepatic failure mice. J Hepatol [Internet]. 2006 Jun 1 [cited 2019 Oct 1];44(6):1105–14. Available from: https://www.sciencedirect.com/science/article/pii/S0168827805006781

77. Arii S, Mise M, Harada T, Furutani M, Ishigami S, Niwano M, et al. Overexpression of matrix metalloproteinase 9 gene in hepatocellular carcinoma with invasive potential. Hepatology [Internet]. 1996 Aug 1 [cited 2019 Sep 11];24(2):316–22. Available from: https://www.sciencedirect.com/science/article/pii/S0270913996003254

78. Nart D, Yaman B, Yılmaz F, Zeytunlu M, Karasu Z, Kılıç M. Expression of MMP-9 in predicting prognosis of hepatocellular carcinoma after liver transplantation. Liver Transplant [Internet]. 2010 May 1 [cited 2019 Sep 11];16(5):NA-NA. Available from: http://doi.wiley.com/10.1002/lt.22028

79. Sun M-H, Han X-C, Jia M-K, Jiang W-D, Wang M, Zhang H, et al. Expressions of inducible nitric oxide synthase and matrix metalloproteinase-9 and their effects on angiogenesis and progression of hepatocellular carcinoma. World J Gastroenterol [Internet]. 2005 [cited 2019 Sep 11];11(38):5931. Available from: http://www.wjgnet.com/1007-9327/full/v11/i38/5931.htm

80. Garcia-Irigoyen O, Carotti S, Latasa MU, Uriarte I, Fernández-Barrena MG, Elizalde M, et al. Matrix metalloproteinase-10 expression is induced during hepatic injury and plays a fundamental role in liver tissue repair. Liver Int [Internet]. 2014 Aug 1 [cited 2019 Oct 1];34(7):e257–70. Available from: http://doi.wiley.com/10.1111/liv.12337

81. Pellicoro A, Aucott RL, Ramachandran P, Robson AJ, Fallowfield JA, Snowdon VK, et al. Elastin accumulation is regulated at the level of degradation by macrophage metalloelastase (MMP-12) during experimental liver fibrosis. Hepatology [Internet]. 2012 Jun 1 [cited 2019 Oct 2];55(6):1965–75. Available from: http://doi.wiley.com/10.1002/hep.25567

82. Madala SK, Pesce JT, Ramalingam TR, Wilson MS, Minnicozzi S, Cheever AW, et al. Matrix metalloproteinase 12-deficiency augments extracellular matrix degrading metalloproteinases and attenuates IL-13-dependent fibrosis. J Immunol [Internet]. 2010 Apr 1 [cited 2019 Oct 2];184(7):3955–63. Available from:

http://www.ncbi.nlm.nih.gov/pubmed/20181883

83. Yata Y, Takahara T, Furui K, Zhang LP, Watanabe A. Expression of matrix metalloproteinase-13 and tissue inhibitor of metalloproteinase-1 in acute liver injury. J Hepatol [Internet]. 1999 Mar 1 [cited 2019 Oct 2];30(3):419–24. Available from: https://www.sciencedirect.com/science/article/pii/S0168827899801007

84. Uchinami H, Seki E, Brenner DA, D'Armiento J. Loss of MMP 13 attenuates murine hepatic injury and fibrosis during cholestasis. Hepatology [Internet]. 2006 Aug 1 [cited 2019 Oct 2];44(2):420–9. Available from: http://doi.wiley.com/10.1002/hep.21268

85. George J, Tsutsumi M, Tsuchishima M. MMP-13 deletion decreases profibrogenic molecules and attenuates *N* -nitrosodimethylamine-induced liver injury and fibrosis in mice. J Cell Mol Med [Internet]. 2017 Dec 1 [cited 2019 Oct 2];21(12):3821–35. Available from: http://doi.wiley.com/10.1111/jcmm.13304

86. Prystupa A, Szpetnar M, Boguszewska-Czubara A, Grzybowski A, Sak J, Załuska W. Activity of MMP1 and MMP13 and amino acid metabolism in patients with alcoholic liver cirrhosis. Med Sci Monit [Internet]. 2015 Apr 7 [cited 2019 Oct 3];21:1008–14. Available from: http://www.ncbi.nlm.nih.gov/pubmed/25863779

87. Fallowfield JA, Mizuno M, Kendall TJ, Constandinou CM, Benyon RC, Duffield JS, et al. Scar-associated macrophages are a major source of hepatic matrix metalloproteinase-13 and facilitate the resolution of murine hepatic fibrosis. J Immunol [Internet]. 2007 Apr 15 [cited 2019 Oct 2];178(8):5288–95. Available from: http://www.ncbi.nlm.nih.gov/pubmed/17404313

88. Calabro SR, Maczurek AE, Morgan AJ, Tu T, Wen VW, Yee C, et al. Hepatocyte Produced Matrix Metalloproteinases Are Regulated by CD147 in Liver Fibrogenesis. Ahlenstiel G, editor. PLoS One [Internet]. 2014 Jul 30 [cited 2019 Sep 11];9(7):e90571. Available from: https://dx.plos.org/10.1371/journal.pone.0090571

89. Hironaka K, Sakaida I, Matsumura Y, Kaino S, Miyamoto K, Okita K. Enhanced Interstitial Collagenase (Matrix Metalloproteinase-13) Production of Kupffer Cell by Gadolinium Chloride Prevents Pig Serum-Induced Rat Liver Fibrosis. Biochem Biophys Res Commun [Internet]. 2000 Jan 7 [cited 2019 Oct 3];267(1):290–5. Available from: https://www.sciencedirect.com/science/article/pii/S0006291X99919101

90. Endo H, Niioka M, Sugioka Y, Itoh J, Kameyama K, Okazaki I, et al. Matrix Metalloproteinase-13 Promotes Recovery from Experimental Liver Cirrhosis in Rats. Pathobiology [Internet]. 2011 [cited 2019 Oct 2];78(5):239–52. Available from: http://www.ncbi.nlm.nih.gov/pubmed/21849805

91. Duarte S, Shen X-D, Fondevila C, Busuttil RW, Coito AJ. Fibronectin-α4β1 Interactions in Hepatic Cold Ischemia and Reperfusion Injury: Regulation of MMP-9 and MT1-MMP via the p38 MAPK Pathway. Am J Transplant [Internet]. 2012 Oct 1 [cited 2019 Oct 4];12(10):2689–99. Available from: http://doi.wiley.com/10.1111/j.1600-6143.2012.04161.x

92. Harada T, Arii S, Mise M, Imamura T, Higashitsuji H, Furutani M, et al. Membrane-type matrix metalloproteinase-1(MT1-MMP) gene is overexpressed in highly invasive hepatocellular carcinomas. J Hepatol [Internet]. 1998 Feb 1 [cited 2019 Oct 4];28(2):231–9. Available from: https://www.sciencedirect.com/science/article/pii/0168827888800102

93. Zhou X, Hovell CJ, Pawley S, Hutchings MI, Arthur MJP, Iredale JP, et al. Expression of matrix metalloproteinase-2 and -14 persists during early resolution of experimental liver fibrosis and might contribute to fibrolysis. Liver Int [Internet]. 2004 Oct [cited 2019 Oct 7];24(5):492–501. Available from: http://doi.wiley.com/10.1111/j.1478-3231.2004.0946.x

94. Butler GS, Will H, Atkinson SJ, Murphy G. Membrane-Type-2 Matrix Metalloproteinase Can Initiate the Processing of Progelatinase A and is Regulated by the Tissue Inhibitors of Metalloproteinases. Eur J Biochem [Internet]. 1997 Mar 1 [cited 2019 Oct 7];244(2):653–7. Available from: http://doi.wiley.com/10.1111/j.1432-1033.1997.t01-1-00653.x

95. Roeb E. Matrix metalloproteinases and liver fibrosis (translational aspects). Matrix Biol [Internet]. 2018 Aug 1 [cited 2019 Sep 3];68–69:463–73. Available from: https://www.sciencedirect.com/science/article/pii/S0945053X17303530

96. Jirouskova M, Zbodakova O, Gregor M, Chalupsky K, Sarnova L, Hajduch M, et al. Hepatoprotective Effect of MMP-19 Deficiency in a Mouse Model of Chronic Liver Fibrosis. Ryffel B, editor. PLoS One [Internet]. 2012 Oct 9 [cited 2019 Oct 7];7(10):e46271. Available from: https://dx.plos.org/10.1371/journal.pone.0046271

97. Mohammed FF, Pennington CJ, Kassiri Z, Rubin JS, Soloway PD, Ruther U, et al. Metalloproteinase inhibitor TIMP-1 affects hepatocyte cell cycle via HGF activation in murine liver regeneration. Hepatology [Internet]. 2005 Apr 1 [cited 2019 Oct 7];41(4):857–67. Available from: http://doi.wiley.com/10.1002/hep.20618

Appendix A – TGF-β SMAD pathway

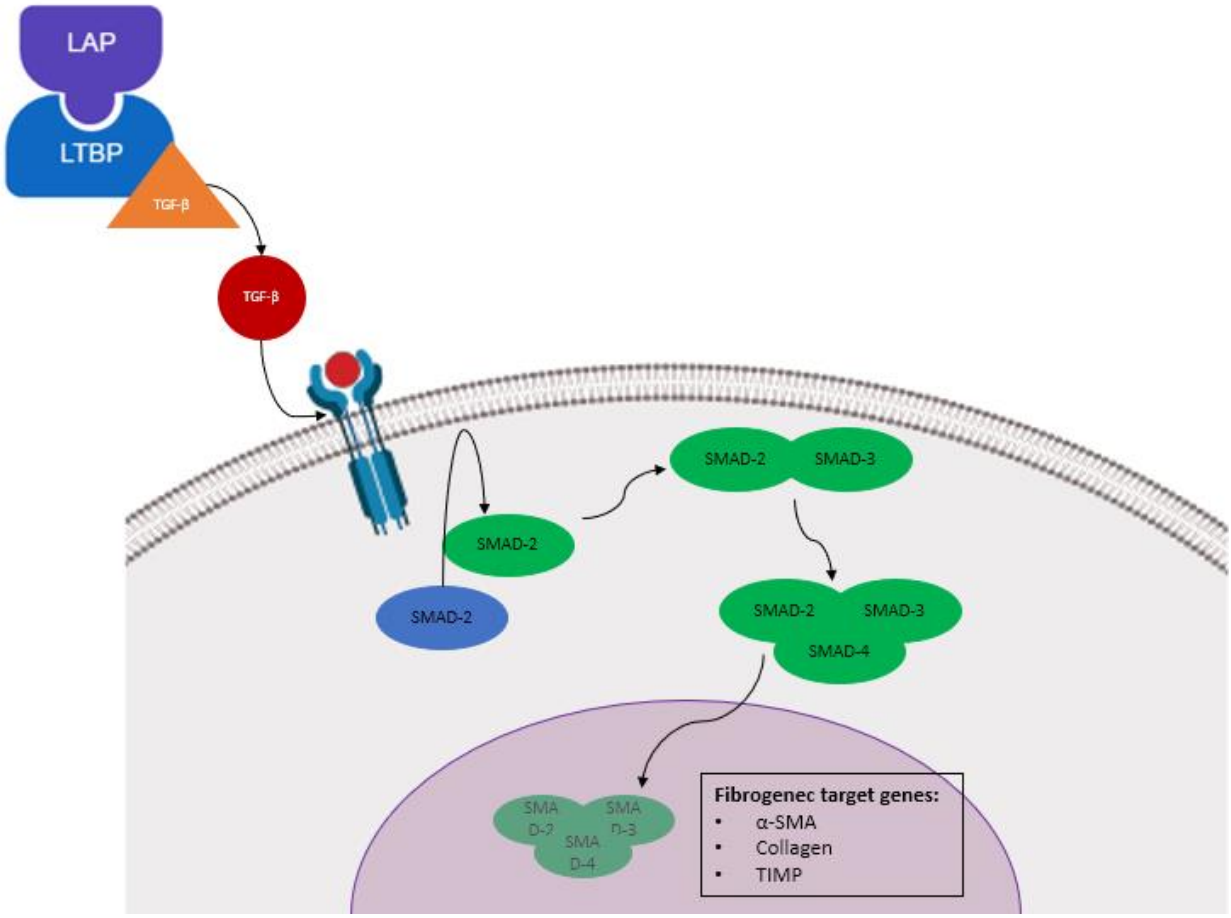

Figure 22. *Latent TGF-β-binding protein (LTBP), which is bound to (inactive) latent TGF-β (orange) and latency-associated peptide (LAP) release activated TGF-β (red). TGF-β binds to TGF-β receptor type II and this receptor activates TGF-β receptor I. This receptor activates SMAD-2 (blue to green). Active SMAD-2 binds with SMAD-3. This in turn binds with SMAD-4. This complex moves to the nucleus and regulate transcription of fibrogenic genes. [Xu, 2016 TGF-b]*

Appendix B – MMPs and their role in Liver diseases

Table 2. *All MMPs with their different function in liver diseases.*

MMP	Group	Roll in Liver disease	Reference
MMP-1	Collagenase	Degrades ECM and thereby attenuates liver fibrosis	(17)
		Decreased expression in histological progression of chronic hepatitis	(53)
MMP-2	Gelatinase	Increased expression in chronic hepatitis induced fibrosis	(54,55)
		Upregulated in HCV induced liver fibrosis and cirrhosis	(54)
		Limits collagen I expression in liver fibrosis	(56)
		Absence supports liver fibrosis	(56,57)
		Serum marker for severity if ALD	(58)
		Expressed during liver regeneration after ischemia/reperfusion (I/R)	(59)
		Increased expression in biliary atresia fibrosis	(60)
MMP-3	Stromelysin	Strongly expressed in HCC, especially in blood vessel adjacent ECM	(61)
		Involved in metastasis regulation during HCC	(62)
		Expressed during inflammation reaction after (I/R)	(59)
MMP-7	Matrilysin	Increased expression in biliary atresia fibrosis	(60)
		Associated with colorectal cancer liver metastasis	(63)
		Serum biomarker for advanced fibrosis	(64)
		Upregulated during oval cell-mediated regeneration	(65)
MMP-8	Collagenase	Viral adeno MMP-8 overexpression ameliorates cirrhosis	(66)
		Activity correlates with repairment of cholestatic liver injury	(67)
		Regulates leukocyte infiltration in resolution of TNF-induces acute hepatitis	(68)
		Serum biomarker for advanced ALD induced liver cirrhosis	(58)
MMP-9	Gelatinase	Induces liver regeneration after partial hepatectomy	(69)
		Induce activated HSC apoptosis	(70)
		Upregulated by infiltrated leukocytes in I/R	(71)
		Leukocyte recruitment and activation in I/R	(72–74)
		Downregulation of MMP-9 inhibits I/R injury	(72,74)
		Promotes brain extravasation and edema in fulminant liver failure (FLF)	(75,76)
		Inhibition of MMP-9 decreases brain injury in FLF	(75)
		Promotes tumor invasion and metastases of HCC	(77,78)
		Biomarker for HCC prognosis	(79)
		Serum marker for advanced ALD induced liver cirrhosis	(58)
MMP-10	Stromelysin	Strongly expressed in HCC, especially in blood vessel adjacent ECM	(61)
		Promotes hepatic wound healing after partial hepatectomy and bile duct ligation	(80)
MMP-11	Stromelysin	Expressed in a later stage of liver regeneration	(59)
		Upregulated in the early stage of HCV induced liver fibrosis	(54)
MMP-12	Others	Roll in ischemia-induced Kupffer cell migration and activation after I/R	(59)
		Regulates elastin degradation in liver fibrosis	(81)
		Inhibits MMP regulated ECM degradation in fibrosis; deficiency attenuates fibrosis	(82)
MMP-13	Collagenase	Elevated expression during acute liver injury	(83)
		Accelerates fibrogenesis in cholestatic livers via initiation of inflammation	(84)
		Promotes GF expression and thereby fibrosis progression in early stage LF	(85)
		Serum marker for ALD induced liver cirrhosis	(86)

		Upregulated in the early stage of HCV induced liver fibrosis Helps degrading ECM and thereby attenuates LF Overexpression accelerates LF recovery by hepatocytes GF stimulation and ECM degradation by MMP-2 and MMP-9 stimulation	(54) (87–89) (90)
MMP-14	Membrane-type MMP	Stimulates recruitment of macrophages in cold IR injury Involved in the invasion potential of HCC Activates MMP-2 thereby leading to fibrolysis	(91) (92) (55,93)
MMP-15	Membrane-type MMP	Can activate MMP-2 Down regulated after partial hepatectomy	(94) (9)
MMP-16	Membrane-type MMP	Expressed in hepatitis, HCC and cirrhosis	(9,95)
MMP-19	Stromelysin	Deficiency lowers response to TGF-β and promotes fibrolysis	(96)
MMP-23	Other	Upregulated in oval cell regulated liver regeneration	(65)
MMP-24	Matrilysin	Upregulated in oval cell regulated liver regeneration Expressed 48h after partial hepatectomy	(65) (97)
MMP-25	Membrane-type MMP	Involved in tumor invasion by MMP activation	(9)
MMP-28	Other	Upregulated in ALD induced inflammation progression and hepatocyte damage	(9)

Appendix C – Primer specification

Table 3. *Specification of used primers; primer name, forward and reverse, melting temperature, GC content and accessions number.*

Primer	**Forward** **Reverse**	**Tm**	**GC%**	**Accessions number**
Col 1α1 human	GTACTGGATTGACCCCAACC CGCCATACTCGAACTGGAAT	57,88/57,77	55,0/50,0	NM_000088.3
Col 3α1 human	AAGAAGGCCCTGAAGCTGAT GTGTTTCGTGCAACCATCCT	59,00/59,05	50/50	NM_000090
α-SMA human	CCCCATCTATGAGGGCTATG CAGTGGCCATCTCATTTTCA	56,61/56,01	55,0/45,0	NM_001613.2
TIMP1 human	GGGGACACCAGAAGTCAACC GGGTGTAGACGAACCGGATG	60,25/60,18	60,0/60,0	NM_003254.2
MMP1 human	TGGTGTCTCACAGCTTCCCA CTCCACATCTGGGCTGCTTC	61,05/60,75	55/60	NM_002421.3
GAPDH human	TCCAAAATCAAGTGGGGCGA TGATGACCCTTTTGGCTCCC	59,89/59,96	50/55	NM_001256799.1
RPS18 human	TGAGGTGGAACGTGTGATCA CCTCTATGGGCCCGAATCTT	58,96/58,94	50/55	NM_022551.2